125 (2024) 205289

Contents lists available at ScienceDirect

Gas Science and Engineering

journal homepage: www.journals.elsevier.com/gas-science-and-engineering

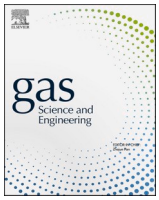

Improved saturation-pressure relationship and multiphase pseudo-pressure calculations for retrograde gas reservoir production under boundary-dominated flow

Kien Tran [a,*], Bright Odike [b], Jonathan Garcez [b], Luis F. Ayala H [b]

[a] Faculty of Petroleum and Energy, Hanoi University of Mining and Geology, Hanoi, Viet Nam
[b] John and Willie Leone Family Department of Energy and Mineral Engineering, The Pennsylvania State University, State College, PA, 16801, United States

A B S T R A C T

For reservoirs containing fluids with complex flow characteristics, the calculation of multiphase pseudo-pressure plays a significant role in production data analysis (PDA) practices. In the case of retrograde gas reservoirs/gas condensate reservoirs under multiphase flow conditions, the lack of a reliable and complete saturation-pressure (S_o-p) relationship presents a significant challenge in obtaining the appropriate value of multiphase pseudo-pressure. Gas condensate reservoirs are one of the viable and lower-emission hydrocarbon sources for meeting the ever-increasing global energy demand. The economic value of producing gas condensates has inspired numerous research into employing innovative production techniques in developing gas condensate fields. Hence, this study proposes an improved saturation-pressure relationship alongside a Fractional Phase Mobility (FPM) criterion to mitigate potential errors in the multiphase pseudo-pressure calculation for gas condensate reservoirs under boundary-dominated flow. This work introduces an improved S_o-p relationship derived using a Rescaled Constant Volume Depletion (CVD) method for estimating multiphase pseudo-pressures. To demonstrate the effectiveness of the proposed approach, we provide direct comparisons with the Classical CVD method and numerical simulation results for multiple gas condensate cases subjected to constant and variable bottomhole pressure (BHP) schedules. In contrast to the classical approach, the Rescaled CVD method consistently delivers superior performance for multiphase pseudo-pressure estimations across all cases, thus supporting its potential as a robust and accurate approach for gas condensate reservoir modeling.

1. Introduction

Production data analysis methods are widely employed to quantitatively analyze rate and pressure signatures from producing wells. These methods are routinely derived via closed-form empirical and/or analytical solutions of the associated governing fluid flow equations. Original gas in place (OGIP), reservoir permeability, and estimated ultimate recovery (EUR) are examples of information acquired using PDA techniques. For single-phase (dry) gas reservoirs, the derivation of analytical methods often relies on linearization techniques such as pseudo-pressure (Al-Hussainy et al., 1966) and pseudo-time (Agarwal, 1979). The application of pseudo-variables transforms the underlying nonlinear gas flow equation to a linear partial differential equation, which can be solved with existing methods previously employed for slightly compressible fluid flow. To eliminate the necessity of customarily using the pseudo-function concept in natural gas engineering analysis, Ye and Ayala H (2012) implemented a straight-forward transformation of pseudo-pressure to a dimensionless density-diffusivity approximation in terms of viscosity-compressibility ratio and density changes to alternatively describe the unsteady behavior of gas reservoirs producing under constant pressure or rate production constraints. Analysis of gas condensate reservoirs exhibits significant differences from dry gas reservoirs, particularly due to the complexity involved in the fluid characterization and multiphase flow effects. Behmanesh et al. (2017) elucidated the unusual behavior in reservoir fluids specific to retrograde gas reservoir production as pressures decreases isothermally below the dew-point pressure and condensate dropout occurs. However, the derivation of analytical models for this type of system still relies on what is called multiphase pseudo-pressure and pseudo-time, which incorporate the nonlinearities associated with pressure (fluid properties) and saturation (relative permeabilities) (Camacho and Raghavan, 1989; Sureshjani and Gerami, 2011). Likewise single-phase gas flow modeling, multiphase pseudo-variables are employed to fully linearize the set of multiphase governing equations and enable the development of closed-form analytical solutions. In fact, Behmanesh et al. (2018) acknowledges that the complex characteristic of two-phase flow prevents a straight implementation of the developed analytical solution because these methods are solely based on single-phase flow assumption.

The decision to employ multiphase pseudo-variables poses addi-

* Corresponding author.
E-mail addresses: tranhuukien@humg.edu.vn (K. Tran), beo5102@psu.edu (B. Odike), jonathan.sgarcez@gmail.com (J. Garcez), ayala@psu.edu (L.F. Ayala H).

https://doi.org/10.1016/j.jgsce.2024.205289
Received 25 November 2023; Received in revised form 15 February 2024; Accepted 19 March 2024
Available online 25 March 2024

tional closure issues due to the inherent relationship between pressure and saturation (Walsh and Lake, 2003). Contrary to single-phase gas pseudo-pressure, multiphase pseudo-pressure also incorporates terms that are dependent on saturation, i.e., relative permeability of gas and condensate (oil) phases. It integrates the entire nonlinear coefficient presented in the flux term of the underlying nonlinear governing equation with respect to pressure. As a result, a saturation-pressure (S_o-p) relationship must be known and available a priori to relate the relative permeabilities functions, which are saturation dependent, to reservoir pressure. A significant body of research has been devoted to properly addressing and developing S_o-p relationships that can closely mimic the in-situ gas condensate behavior during depletion. To evaluate the performance of liquid-rich gas wells, O'Dell (1967) proposed the use of two-phase pseudo-pressure to account for gas dissolved in condensate during depletion. Jones and Raghavan (1988) established an important relationship between pressure and saturation in multiphase flow reservoirs. In a two-phase region, relative permeability of each phase also heavily depends on fluid saturation. Fevang and Whitson (1996) pointed out that liquid banking occurring around the near-wellbore region severely affects the well deliverability of gas condensate reservoirs. In the same work, the authors proposed a new method to calculate the two-phase pseudo-pressure drawdown, Δm_{tp}, and the Δm_{tp} calculation is divided into three regions upon phase distribution and mobility. The multiphase pseudo-pressure calculation proposed by Fevang and Whitson (1996) employed a pressure-saturation relationship acquired from the producing gas-oil-ratio and Constant Volume Depletion (CVD) data. Sureshjani and Gerami (2011) introduced the two-phase pseudo-time concept, presenting a well performance model in direct association with a single-phase gas model.

Among the primary purposes of PDA for multiphase flow systems, reserve estimation plays a crucial role in decision-making for economically viable reservoir development. Cheng et al. (2008) investigated how uncertainty changes in reserve estimation by analyzing near-abandonment oil and gas wells as more production data become available. Zhang and Ayala (2014a) demonstrated that the rescaled exponential equations in the density-based approach apply to model gas-rate decline in boundary-dominated flow for constant bottomhole pressure specifications. Zhang and Ayala (2014b) also illustrated the effectiveness of the density-based approach in analyzing boundary-dominated gas production data analysis of variable-pressure-drawdown and variable-rate systems. Zhang and Ayala (2016) presented the density-based straight-line analysis to obtain the OGIP of gas condensate reservoirs from the reciprocal of the slope of a straight line, by plotting the rescaled production rate versus the rescaled cumulative production. Behmanesh et al. (2018) presented an expansion of the single-phase flowing material balance model, capable of estimating OGIP by fitting a straight line through the normalized flow rate and cumulative production. Sun and Ayala (2020) extended the density-based approach, previously developed for liquid-rich gas systems, to determine the original fluid in place of an oil/water system. The above-mentioned approaches employed the well-known concepts of tank material balance and multiphase pseudo-pressure. The key challenge in these inverse analyses is that multiphase pseudo-pressure calculation requires information on average reservoir pressure and saturation-pressure distribution at reservoir conditions, which are not readily available. Thus, the implementation of current inverse models must incorporate certain assumptions for saturation-pressure relationships as well as an iterative protocol to achieve appropriate reserve values. This study aimed to investigate the drawdown behavior of conventional gas condensate systems under boundary-dominated flow.

Panja et al. (2020) emphasized that developing an analytical model entails understanding the flow mechanisms of gas condensate fluids in porous media. As mentioned earlier, multiphase pseudo-pressure plays a pivotal role in developing analytical PDA methods. Therefore, this work's main objective is to present an improved saturation-pressure profile to overcome the complication in calculating multiphase pseudo-pressure due to the lack of a complete S_o-p relationship in gas condensate reservoirs. Because of its focus on boundary-dominated flow, the scope of this study is conventional retrograde gas reservoirs where capillary pressure effects are considered negligible. In unconventional reservoirs such as shale or tight formations, however, capillary pressure can play a significant role in fluid behavior due to the small pore sizes, and different models are needed given the presence of infinite-acting flow (Zhang and Ayala, 2017, 2019; Zhang et al., 2020). The proposed method attempts to obtain the S_o-p profile through a Rescaled CVD approach directly. As part of the improved S_o-p profile, we introduce the Fractional Phase Mobility (FPM) concept to define a new upper bound pressure for the steady-state flow region in a gas condensate reservoir. With the goal of verifying its robustness, we evaluated the accuracy of multiphase pseudo-pressure calculations using the traditional method (Classical CVD method) and the proposed method (Rescaled CVD method) through the validation of multiple case studies.

2. Theoretical background

In this study, we utilize the compositionally-extended black-oil (CEBO) model (Ertekin and Ayala, 2018) to set up the governing equation for a gas condensate reservoir. When considering a waterless hydrocarbon system, the CEBO model specifically contains only two pseudo-components (O, G) and two reservoir phases (oil and gas phase). Given the thermodynamic nature of a binary mixture ($N_c = 2$), the flash calculation could be executed non-iteratively using standard black-oil PVT properties (B_o, B_g, R_s and R_v) at each prevailing pressure value. For such a system, the governing flow equation for surface gas and surface oil components can be expressed as Eq. (1) and Eq. (2), respectively:

$$\nabla\cdot\left(\left(\omega_{Gg}\rho_g\frac{k_{rg}}{\mu_g}+\omega_{Go}\rho_o\frac{k_{ro}}{\mu_o}\right)\nabla p\right)=\frac{\varphi}{k}\frac{\partial}{\partial t}\left(S_g\omega_{Gg}\rho_g+S_o\omega_{Go}\rho_o\right) \tag{1}$$

$$\nabla\cdot\left(\left(\omega_{Oo}\rho_o\frac{k_{ro}}{\mu_o}+\omega_{Og}\rho_g\frac{k_{rg}}{\mu_g}\right)\nabla p\right)=\frac{\varphi}{k}\frac{\partial}{\partial t}\left(S_o\omega_{Oo}\rho_o+S_g\omega_{Og}\rho_g\right) \tag{2}$$

where ρ_g and ρ_o are the gas and oil phase densities at reservoir condition, and can be related to PVT parameters as:

$$\rho_g=\frac{\rho_{gsc}+\alpha_c\rho_{osc}R_v}{\alpha_c B_g} \tag{3}$$

$$\rho_o=\frac{\alpha_c\rho_{osc}+\rho_{gsc}R_s}{\alpha_c B_o} \tag{4}$$

ω_{Gg} and ω_{Go} are mass concentrations of surface gas component in reservoir gas phase and oil phase, respectively:

$$\omega_{Gg}=\frac{\rho_{gsc}\frac{V_g}{B_g}}{\alpha_c\rho_g V_g}=\frac{\rho_{gsc}}{\rho_g B_g} \tag{5a}$$

$$\omega_{Go}=\frac{\rho_{gsc}R_s\frac{V_o}{B_o}}{\alpha_c\rho_o V_o}=\frac{\rho_{gsc}R_s}{\rho_o B_o} \tag{5b}$$

Similarly, ω_{Og} and ω_{Oo} are mass concentrations of surface oil component in reservoir gas phase and oil phase, respectively:

$$\omega_{Og}=\frac{\alpha_c\rho_{osc}R_v\frac{V_g}{B_g}}{\alpha_c\rho_g V_g}=\frac{\rho_{osc}R_v}{\rho_g B_g} \tag{6a}$$

$$\omega_{Oo}=\frac{\alpha_c\rho_{osc}\frac{V_o}{B_o}}{\alpha_c\rho_o V_o}=\frac{\rho_{osc}}{\rho_o B_o} \tag{6b}$$

In PDA application for a dry-gas reservoir, pseudo-pressure stands as a key element for the linearization of the governing PDE and subsequent

derivation of linear-like solution. In the same extent, multiphase pseudo-pressure lays the ground for multiphase PDA by providing means to linearize Eqs. (1) and (2). Multiphase pseudo-pressure considers the effect of varying wellstream composition, and it can be defined for a gas condensate reservoir as:

$$\Delta m_g(p) = m_g(\bar{p}) - m_g(p_{wf}) = \int_{p_{wf}}^{\bar{p}} \left(\omega_{Gg}\rho_g\frac{k_{rg}}{\mu_g} + \omega_{Go}\rho_o\frac{k_{ro}}{\mu_o}\right)dp \tag{7}$$

$$\Delta m_o(p) = m_o(\bar{p}) - m_o(p_{wf}) = \int_{p_{wf}}^{\bar{p}} \left(\omega_{Oo}\rho_o\frac{k_{ro}}{\mu_o} + \omega_{Og}\rho_g\frac{k_{rg}}{\mu_g}\right)dp \tag{8}$$

The primary challenge when adopting multiphase pseudo-pressure approach is directly associated with the limited knowledge of saturation-pressure relationship since all the parameters in Eq. (7) and Eq. (8) depend solely upon these two variables.

Classical method of multiphase pseudo-pressure calculation.

Originally proposed by Fevang and Whitson (1996), the classical method segregated the multiphase pseudo-pressure calculation into three integrals, representing three flow regions spreading from bottomhole flowing pressure p_{wf} to average reservoir pressure $\bar{p}$. Fig. 1 graphically portrays these flow regions in a gas condensate reservoir with distinct phase behavior and relative permeability.

Region I is a two-phase flow region exhibiting a steady-state flow where both the gas and condensate phases are mobile. This region appears near the wellbore spreads from p_{wf} to p^*. The value p^* serves as an upper pressure bound for Region I at which the oil saturation crosses a critical value ($S_o|_{p*} > S_{oc}$). Thus, oil phase and gas phase start flowing concurrently. The pseudo-pressure difference in this region is expressed as:

$$\Delta m_{g,I}(p) = m_{g,I}(p^*) - m_{g,I}(p_{wf}) = \int_{p_{wf}}^{p^*} \left(\omega_{Gg}\rho_g\frac{k_{rg}}{\mu_g} + \omega_{Go}\rho_o\frac{k_{ro}}{\mu_o}\right)dp \tag{9a}$$

$$\Delta m_{o,I}(p) = m_{o,I}(p^*) - m_{o,I}(p_{wf}) = \int_{p_{wf}}^{p^*} \left(\omega_{Oo}\rho_o\frac{k_{ro}}{\mu_o} + \omega_{Og}\rho_g\frac{k_{rg}}{\mu_g}\right)dp \tag{9b}$$

The characteristic of steady-state flow granted a constant gas-oil ratio (GOR) across Region I, meaning that the producing GOR recorded at surface could be assigned for any pressure value in between p_{wf} and p^* when tubing effect and temperature gradient are negligible (Fetkovich et al., 1986):

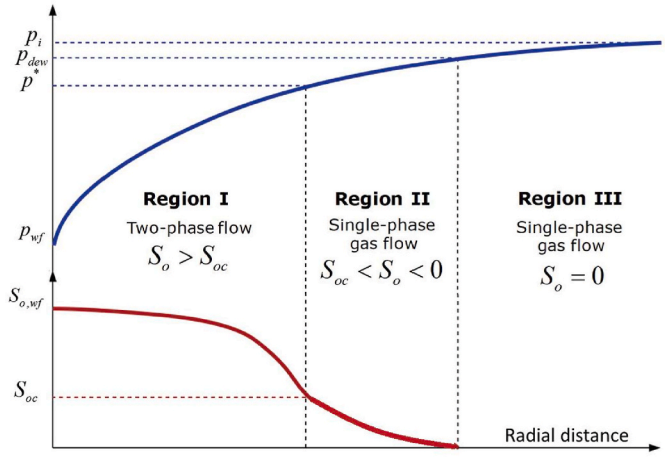

Fig. 1. Three flow regions in a producing gas condensate reservoir.

$$GOR = \frac{q_{gsc}}{q_{osc}} = \frac{\rho_{osc}}{\rho_{gsc}}\frac{kA\left[\gamma_{gsc}\frac{\partial p}{\partial r}\right]_{r=0}}{kA\left[\gamma_{osc}\frac{\partial p}{\partial r}\right]_{r=0}} = \frac{\rho_{osc}}{\rho_{gsc}}\left(\frac{\omega_{Gg}\rho_g\frac{k_{rg}}{\mu_g} + \omega_{Go}\rho_o\frac{k_{ro}}{\mu_o}}{\omega_{Oo}\rho_o\frac{k_{ro}}{\mu_o} + \omega_{Og}\rho_g\frac{k_{rg}}{\mu_g}}\right)\Bigg|_{r=0} \tag{10}$$

where A is drainage area, γ_{gsc} and γ_{osc} is the mobility of surface gas and surface oil component, respectively:

$$\gamma_{gsc} = \omega_{Gg}\rho_g\frac{k_{rg}}{\mu_g} + \omega_{Go}\rho_o\frac{k_{ro}}{\mu_o} \tag{11}$$

$$\gamma_{osc} = \omega_{Oo}\rho_o\frac{k_{ro}}{\mu_o} + \omega_{Og}\rho_g\frac{k_{rg}}{\mu_g} \tag{12}$$

Eq. (10) could be re-written as Eq. (13) to constitute the saturation-pressure relationship for Region I. The left-hand side (LHS) of Eq. (11) is saturation dependent while the right-hand side RHS can be calculated using PVT and producing GOR data. Thus, the oil saturation can be determined by a simple table-look up procedure since each value of the ratio $\frac{k_{ro}}{k_{rg}}$ yields a unique value of S_o from relative permeability data table.

$$\frac{k_{ro}}{k_{rg}}\Bigg|_{S_{o,wf}\to S_{oc}} = \left(\frac{1 - GOR{\cdot}R_v}{GOR - R_s}\right)\frac{\mu_o B_o}{\mu_g B_g}\Bigg|_{p_{wf}\to p^*} \tag{13}$$

The convenient form of Eq. (13) enables the development of a proper relationship of how pressure and saturation are correlated within the interval, $p_{wf} < p \le p^*$. The ratio k_{rg}/k_{ro} is solely dependent on PVT data (B_o, B_g, R_s, R_v), which is readily available for the fluid of interest. This pressure-dependent ratio is uniquely linked to saturation using relative permeability curves (k_{ro} and k_{rg} as a function of S_o) (Evinger and Muskat, 1942).

Region II is the accumulation or condensate build-up region where condensate droplet starts to appear at the upper pressure bound p_{dew} and liquid saturation continues increasing up to critical value at p^*. As pressure depletes from p^* to p_{dew}, the liquid phase remains immobile and pseudo-pressure drawdown is specifically related to gas phase's mobility:

$$\Delta m_{g,II}(p) = m_{g,II}(p_{dew}) - m_{g,II}(p^*) = \int_{p^*}^{p_{dew}} \left(\omega_{Gg}\rho_g\frac{k_{rg}}{\mu_g}\right)dp \tag{14a}$$

$$\Delta m_{o,II}(p) = m_{o,II}(p_{dew}) - m_{o,II}(p^*) = \int_{p^*}^{p_{dew}} \left(\omega_{Og}\rho_g\frac{k_{rg}}{\mu_g}\right)dp \tag{14b}$$

Region III is a representative of a typical undersaturated gas condensate reservoir because the reservoir pressure in this region is higher than the dew-point pressure. When single phase flow of gas is prevailing, flowing composition will remain constant throughout this region, from average reservoir pressure, $\bar{p}$ to lower pressure bound, p_{dew}. The multiphase pseudo-pressure difference in this region perceives identical treatment to pseudo-pressure calculation in a dry-gas reservoir:

$$\Delta m_{g,III}(p) = m_{g,III}(\bar{p}) - m_{g,III}(p_{dew}) = k_{rg}(S_{wc})\int_{p_{dew}}^{\bar{p}} \left(\frac{\rho_g}{\mu_g}\right)dp \tag{15a}$$

$$\Delta m_{o,III}(p) = 0 \tag{15b}$$

It is noted that Region III does not exist if the average reservoir pressure drops below dew-point pressure. In such a case, the upper pressure bound of Region II will be $\bar{p}$ instead of p_{dew}. In summary, the multiphase pseudo-pressure drawdown across the whole flow domain in Eq. (7) and Eq. (8) takes the expanded forms below:

$$\Delta m_g(p) = \int_{p_{wf}}^{p^*} \left(\omega_{Gg}\rho_g\frac{k_{rg}}{\mu_g} + \omega_{Go}\rho_o\frac{k_{ro}}{\mu_o}\right)dp + \int_{p^*}^{p_{dew}} \left(\omega_{Gg}\rho_g\frac{k_{rg}}{\mu_g}\right)dp + k_{rg}(S_{wc})\int_{p_{dew}}^{\bar{p}} \left(\frac{\rho_g}{\mu_g}\right)dp \quad (16a)$$

$$\Delta m_o(p) = \int_{p_{wf}}^{p^*} \left(\omega_{Oo}\rho_o\frac{k_{ro}}{\mu_o} + \omega_{Og}\rho_g\frac{k_{rg}}{\mu_g}\right)dp + \int_{p^*}^{p_{dew}} \left(\omega_{Og}\rho_g\frac{k_{rg}}{\mu_g}\right)dp \quad (16b)$$

It is well-known that the complication in multiphase pseudo-pressure calculation arises from an integral part of Eq. (14a) and Eq. (14b) for Region II since saturation-pressure (S_o-p) relationship in this region remains unknown. The most popular treatment for S_o-p profile in lieu of a rigorous formula is to correlate saturation value in Region II to the amount of liquid drop-out in Constant Volume Depletion (CVD) test.

$$S_o(p) = V_{ro,CVD}(1 - S_{wc}) \quad (17)$$

where $V_{ro,CVD}$ is the fractional amount of liquid dropout in a CVD test and S_{wc} is the irreducible water saturation. Nonetheless, this classical treatment appears ill-suited for many cases. For instance, where multiphase flow is evident based on production data ($S_{o,wf} > S_{oc}$) but CVD data suggested zero oil mobility since the maximum liquid drop-out is less than critical saturation value ($S_{o,\max\ (CVD)} < S_{oc}$).

3. Proposed approach

The definition of pressure bounds and mobile fluid phase(s) in each region and the customary utilization of CVD data are integral components for multiphase pressure calculation in gas condensate reservoirs. In this work, we defined a new upper pressure-bound limit for Region I and an improved methodology for tackling the discontinuity present in the S_o-p transition between Region I and Region II. The proposed model fully captures the effect of phase transition due to retrograde gas condensation, which is one of the mechanisms behind the condensate appearance and accumulation (build-up) around the wellbore region once the pressure drops below dew-point conditions. This phase transition is captured by tracking the changes in the volatilized condensate content, R_v of the flowing gas in the reservoir.

3.1. New upper bound pressure limit for Region I using FPM

The first key element in developing an improved saturation-pressure relationship, and therefore a better pseudo pressure calculation, is the definition of a proper transition between Regions I and II. Routinely, the upper bound pressure of Region I (p^*) is commonly determined by the relationship, $R_v|_{p^*} = 1/GOR$, where p^* represents the pressure value in which the multiphase flow behavior departs from steady-state regime (indicated by the discontinuity of constant GOR behavior in Region I). With the conventional approach, the ratio of k_{rg}/k_{ro} at p^* is forced to be infinite since the oil saturation at p^* is equal to the critical oil saturation, S_{oc}. This dictation leads to a sudden drop in oil saturation when pressure approaching the outer edge of Region I and ultimately results a misrepresentation of fluid behavior in the multiphase environment. Fevang and Whitson (1996) suggested that the upper limit of k_{rg}/k_{ro} should equal 50 for practically all gas condensate because the k_{rg} value is relatively high at $k_{rg}/k_{ro} > 50$ and only a small pressure interval below p^* yield this range of k_{rg}/k_{ro}. However, primary calculation from our case studies indicates an unsatisfactory multiphase pseudo-pressure calculation when imposing a predetermined ratio of $k_{rg}/k_{ro} = 50$ as the upper limit of Region I. At bottomhole pressure, a wide variation of k_{rg}/k_{ro} (between 2 and above 300) is observed due to the broad spectrum of the gas richness and drawdown magnitude in our case studies. This observation indicated that the upper bound of the steady-state flow region should be dynamically estimated in correlation with wellbore condition.

Based on the premise that the concurrent mobility of gas and condensate phases granted a constant in-situ GOR behavior in the steady-state flow region, GOR behavior versus the FPM across the whole pressure domain is investigated. In this study, we established FPM as the relative value of phase mobility ratio across flow domain to the counterpart at wellbore condition, defined as:

$$FPM(p) = \frac{(\gamma_o/\gamma_g)|_p}{(\gamma_o/\gamma_g)|_{p_{wf}}} \quad (18)$$

where $\gamma_o = \frac{k_{ro}}{\mu_o B_o}$ and $\gamma_g = \frac{k_{rg}}{\mu_g B_g}$, are the mobilities of condensate and gas phases, respectively.

Figs. 2–4 display GOR behavior as a function of reservoir pressure for lean, intermediate, and rich gas condensate systems. To investigate the influence of gas composition, three mixtures were defined with controlled proportions of methane (C1) and n-pentane (n-C5): lean gas condensate (90% C1, 10% n-C5), intermediate gas condensate (80% C1, 20% n-C5), and rich gas condensate (75% C1, 25% n-C5). The GOR-pressure envelope with FPM contours is constructed using PVT data, where $GOR_{max} = \frac{1}{R_v}$ and $GOR_{min} = R_s$. The actual GOR paths at several time steps are plotted using the S_o-p profile output from numerical simulation.

As shown in Figs. 2–4, the actual GOR paths evidently departed from constant behavior prior to the commonly defined p^*. Here, the FPM contours serve as an indicative parameter to determine the departure point of GOR path from constant behavior. Noticeably, the majority of GOR profiles start deviating at pressure, p_1, corresponding to the contour of $FPM = 0.1$ and $FPM = 0.2$, in which the mobility ratio of condensate phase over gas phase is equal a tenth to a fifth of the counterpart at wellbore condition. This observation provides additional evidence to support the imperative of identifying an alternative method for establishing the upper limit of the steady-state flow region using FPM as an indicator.

To further validate the p_1 determination protocol using FPM_{p1} criterion and show that the customary assumption of constant GOR in Region I is ill-suited, relationships between $\frac{dGOR}{dp}$ and FPM for all gas condensate cases are exhibited in Fig. 5. The $\frac{dGOR}{dp}$ versus FPM plot is constructed by fitting a polynomial to the GOR vs. pressure trend with emphasis on the transition interval between **Region I** and **Region II** as illustrated in the close-up transition interval in the GOR-pressure envelopes (Figs. 2b, 3b, and 4b). The first derivative of the fitted GOR polynomial with respect to pressure is obtained through the application of central difference approximation.

Traditionally, it is assumed that GOR should be constant in Region I until FPM gets to zero to define the immobility of the condensate phase in Region II. However, the plot of $\frac{dGOR}{dp}$ versus FPM in Fig. 5 further reiterates that the assumption of a constant GOR behavior in Region I should be revised. Although yielding similar proposition in consonance with the GOR-pressure envelopes, the $\frac{dGOR}{dp}$ versus FPM however suggests that FPM is fluid-dependent. Generally, it is observed that deviation from a constant GOR behavior becomes more pronounced at and around a range of FPM of 0.1–0.2 for the distinct gas condensate cases. Nevertheless, sensitivity analyses/preliminary results from inverse modeling and best production/flow rate predictions exercises recapitulate FPM = 0.2 as the most suitable protocol to determine the upper limit pressure p_1 Region I, at which GOR departs from a constant behavior. Based on these observations, it is suggested that the steady-state flow region should be characterized from p_{wf} to p_1, which satisfies the $FPM_{p_1} = 0.2$ criterion.

3.2. Condensate accumulation region (Region II)

As aforementioned, the lack of a saturation-pressure (S_o-p) relationship in Region II enforced the utilization of CVD data for multiphase

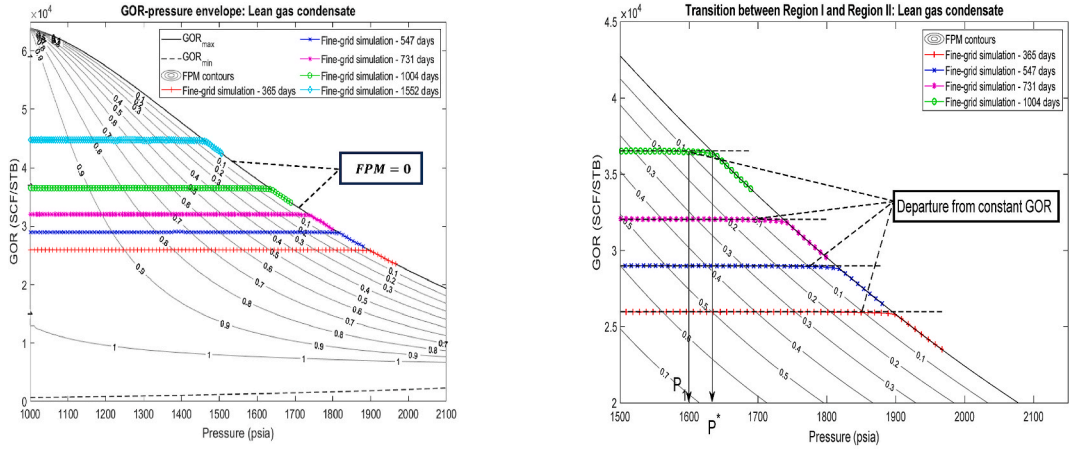

(a) (b)

Fig. 2. GOR behavior – lean gas condensate. (a) Through the total pressure domain (b) through the transition interval between Region I and Region II.

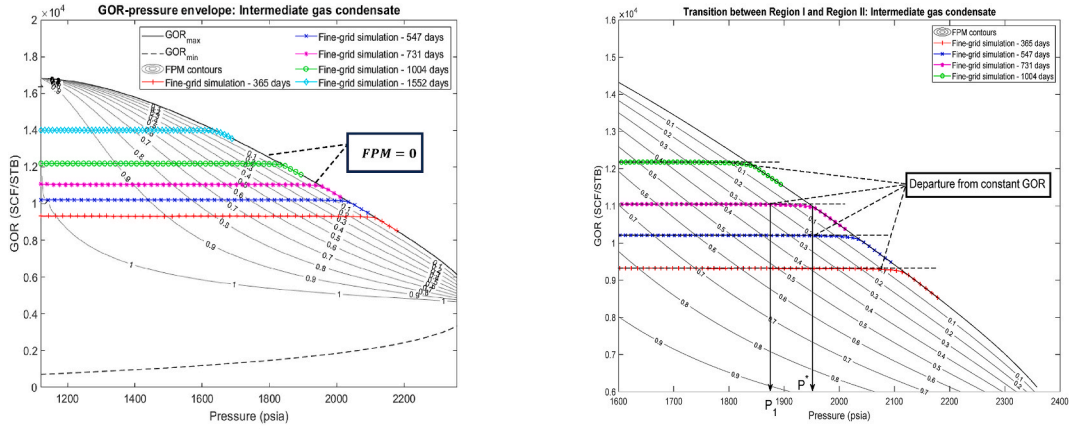

(a) (b)

Fig. 3. GOR behavior – intermediate gas condensate. (a) Through the total pressure domain (b) through the transition interval between Region I and Region II.

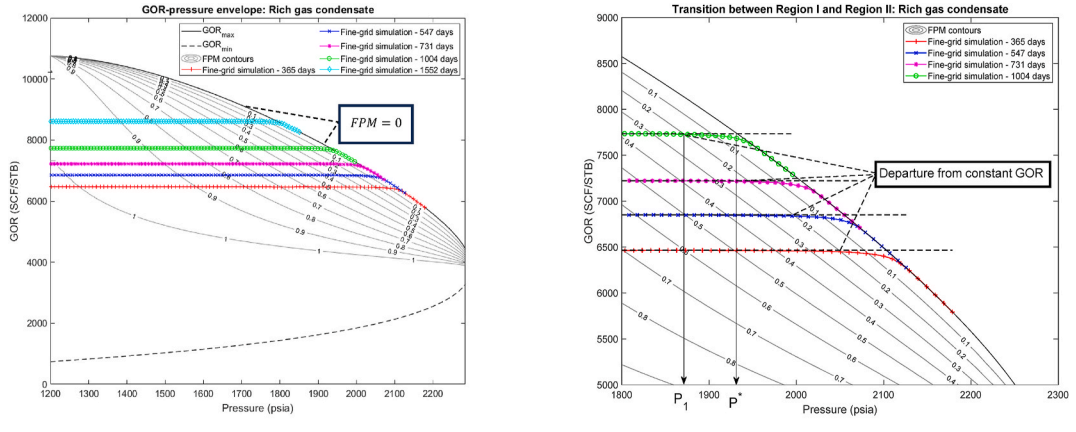

(a) (b)

Fig. 4. GOR behavior – rich gas condensate. (a) Through the total pressure domain (b) through the transition interval between Region I and Region II.

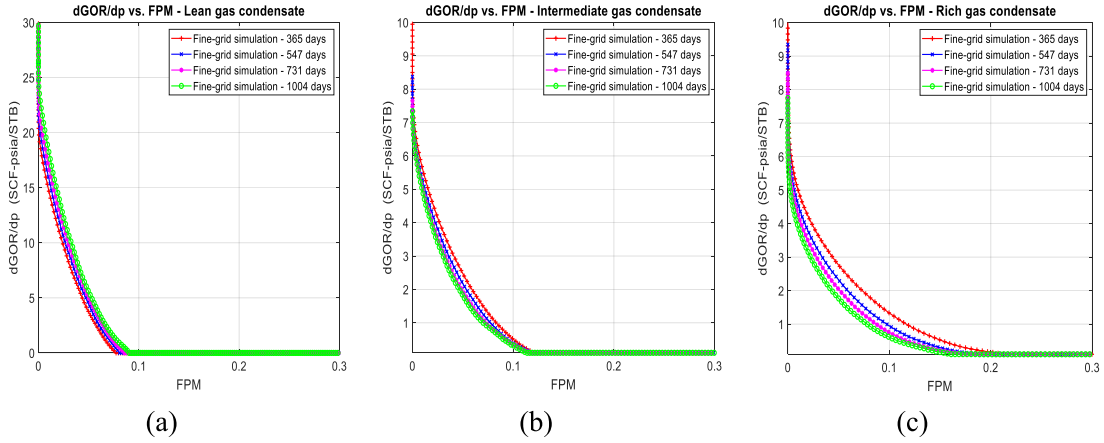

Fig. 5. $\frac{dGOR}{dp}$ vs. *FPM*. (a) Lean gas condensate (b) intermediate gas condensate (c) rich gas condensate.

pseudo-pressure calculation, which was shown to be unsuitable for this practice (Behmanesh et al., 2015; Becker et al., 2016). In this section, we proposed a new method to model condensate build-up in this region by rescaling the available CVD data. In contrast to using CVD data to obtain S_o from p^* to $\bar{p}$, the Rescaled CVD method determines S_o for an arbitrary pressure p in the interval from p_1 to $\bar{p}$ through the following expression:

$$S_{o,rescaled}\big|_p = S_{o,CVD}\big|_p \cdot F_r\big|_p \tag{19}$$

where $F_r|_p$ is the rescaling factor at pressure p, defined as:

$$F_r\big|_p = 1 + \frac{\left(S_o|_{p_1} \Big/ S_{o,CVD}\big|_{p_1} - 1\right)(\bar{p} - p)}{\bar{p} - p_1} \tag{20}$$

where $S_o|_{p_1}$ is the predetermined condensate saturation using a constant GOR approach in Eq. (13). Fig. 6 illustrates the values of the rescaling factor F_r in the pressure interval from p_1 to $\bar{p}$, where F_r versus p followed a simple straight-line relationship between $\left(p_1, S_o|_{p_1} / S_{o,CVD}\big|_{p_1}\right)$ and $(\bar{p}, 1)$. In summary, the proposed S_o-p profile is constructed from the following steps:

1) Determine p_1 using $FPM_{p_1} = 0.2$ criterion.
2) For the steady-state region from p_{wf} to p_1, S_o-p profile is obtained through constant GOR approach using Eq. (13).
3) For pressure interval from p_1 to $\bar{p}$, S_o-p profile is computed with Rescaled CVD approach using Eqs. (19) and (21).

The rescaling factor within a pressure interval of p_1 to $\bar{p}$ yields a straight-line relationship between the $\left(p_1, S_o|_{p_1} \Big/ S_{o,CVD}\big|_{p_1}\right)$ and $(\bar{p}, 1)$ is shown in Fig. 6.

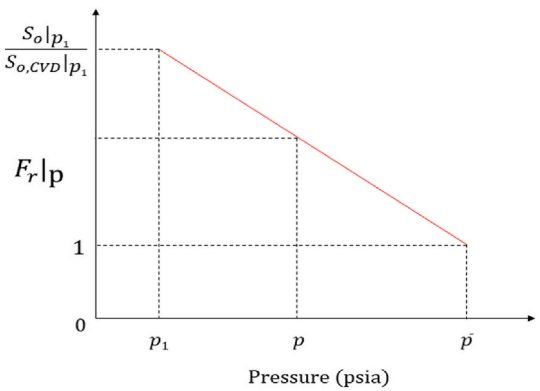

Fig. 6. Rescaling factor, F_r in Eq. 20.

Coupling the proposed FPM and Rescaled CVD methods, the multiphase pseudo-pressure of gas and oil surface components are calculated as follows:

$$m_g(\bar{p}) - m_g(p_{wf}) = \int_{p_{wf}}^{p_1} \left(\omega_{Gg}\rho_g\frac{k_{rg}}{\mu_g} + \omega_{Go}\rho_o\frac{k_{ro}}{\mu_o}\right)dp + \int_{p_1}^{\bar{p}} \left(\omega_{Gg}\rho_g\frac{k_{rg}}{\mu_g}\right)dp \tag{21}$$

$$m_o(\bar{p}) - m_o(p_{wf}) = \int_{p_{wf}}^{p_1} \left(\omega_{Og}\rho_g\frac{k_{rg}}{\mu_g} + \omega_{Oo}\rho_o\frac{k_{ro}}{\mu_o}\right)dp + \int_{p_1}^{\bar{p}} \left(\omega_{Og}\rho_g\frac{k_{rg}}{\mu_g}\right)dp \tag{22}$$

4. Case studies

The primary goal of this section is to compare the proposed methodology against the classical method for multiphase pseudo-pressure calculation. We identify the advantages of the proposed method using results from its implementation on all case studies and benchmarking against numerical simulation output. Three binary mixtures of CH_4 and n-C_5H_{12} are generated by our in-house phase behavior model with different compositions to represent a variety of gas richness. According to Walsh and Lake (2003), producing GOR is the main criterion to classify a gas condensate system which is ranging from 3500 SCF/STB for rich gas to above 30,000 SCF/STB for lean gas. For each type of gas condensate, a synthetic case study is created using a commercial numerical simulator (CMG-IMEX) where the reservoir models are structured as finely discretized radial cylindrical grids of isotropic homogeneity under boundary-dominated flow with a vertical well in the center and production schedule set to be under a constant BHP condition for about 3000 days (7–8 years). The grid blocks assigned to the gas condensate cases are – lean gas (900 × 1 × 1), intermediate gas (650 × 1 × 1), and rich gas (500 × 1 × 1). The relative permeability set is obtained using a modified Corey function. PVT data and input parameters for the employed case studies are detailed in Appendix A and Appendix B respectively. The production history and producing GOR for case 1–3 are provided in Appendix B.

For all case studies, the initial reservoir pressures are set to be equal to the dew-point pressures of the mixtures to induce two-phase flow condition at early time. The CVD data for all three gas condensate samples are shown in Fig. 7, and indicate the maximum liquid dropout are 5%, 16% and 24% for lean, intermediate, and rich gas, respectively. The phase envelopes of these mixtures are depicted in Fig. 8, show how the composition directly decided the state of the fluid samples at any

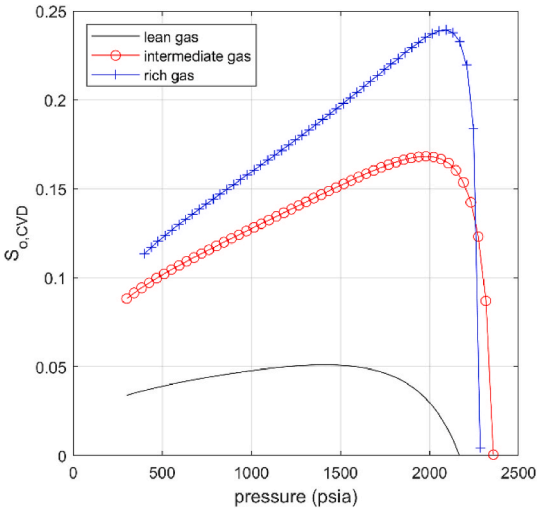

Fig. 7. CVD data.

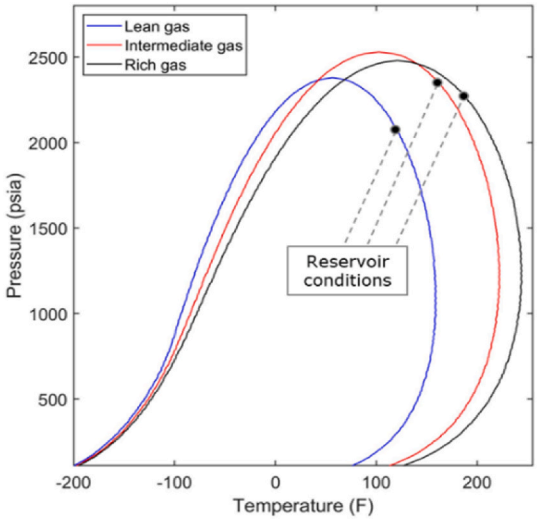

Fig. 8. Phase envelope of gas condensate samples on p-T diagram.

specific reservoir condition. As the composition of light component (C1 or CH_4) gradually decreases from 90% to 80% then 75%, the richness level of gas increases and pushes the phase envelope to the right, where the fluid system requires higher temperature to be completely evaporated.

The direct comparisons of S_o-p profiles produced by fine-grid simulation, the classical method, and the proposed method are provided in Appendix E. The performance comparisons in estimating multiphase pseudo-pressure for the surface gas components are shown in Figs. 9 and 10. Results from the practice of the classical method exhibit lowest overall accuracy across two case studies, further substantiating the fact that CVD data is inadequate to capture the fluid behavior in gas condensate reservoirs. Similar findings can be observed from the comparison of multiphase pseudo-pressure calculation for surface oil components (Figs. 11 and 12). Throughout the evaluation, the proposed S_o-p relationship and multiphase pseudo-pressure calculations from the Rescaled CVD method displayed the most consistent performance, thus corroborating our model as a robust tool in gas condensate reservoir modeling. From the ascertained results, we observed that the average deviation in the multiphase pseudo-pressure calculation is 4–5% for the lean gas condensate system and around 1–2% for the intermediate and rich gas condensate systems.

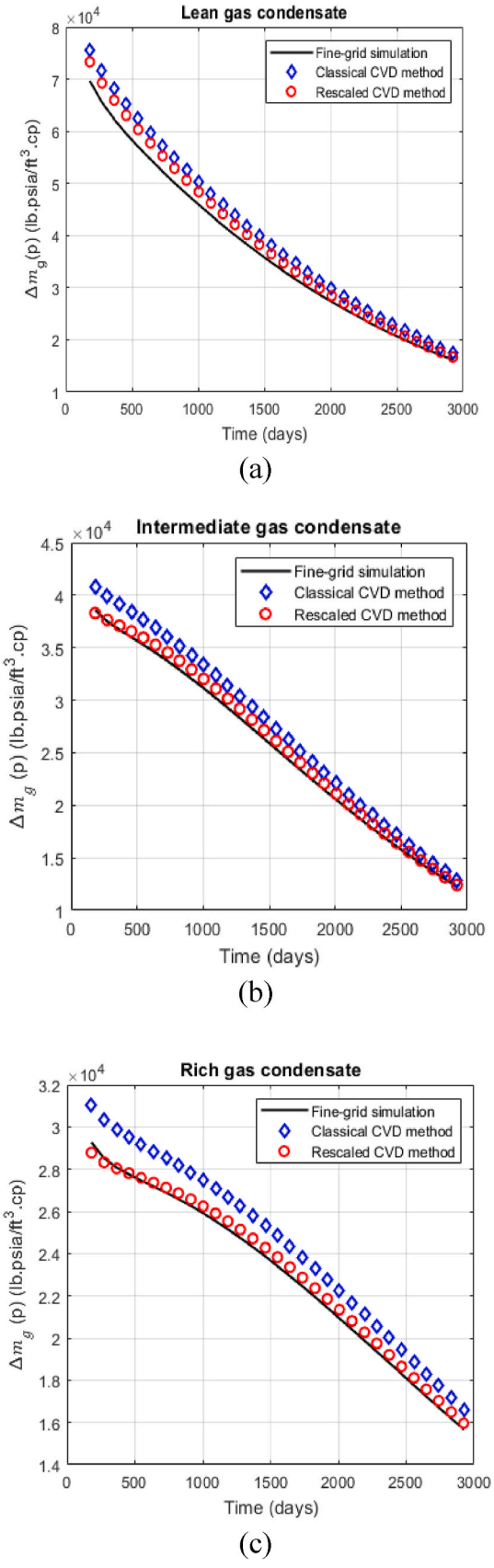

Fig. 9. $\Delta m_g(p)$ comparison – constant BHP.

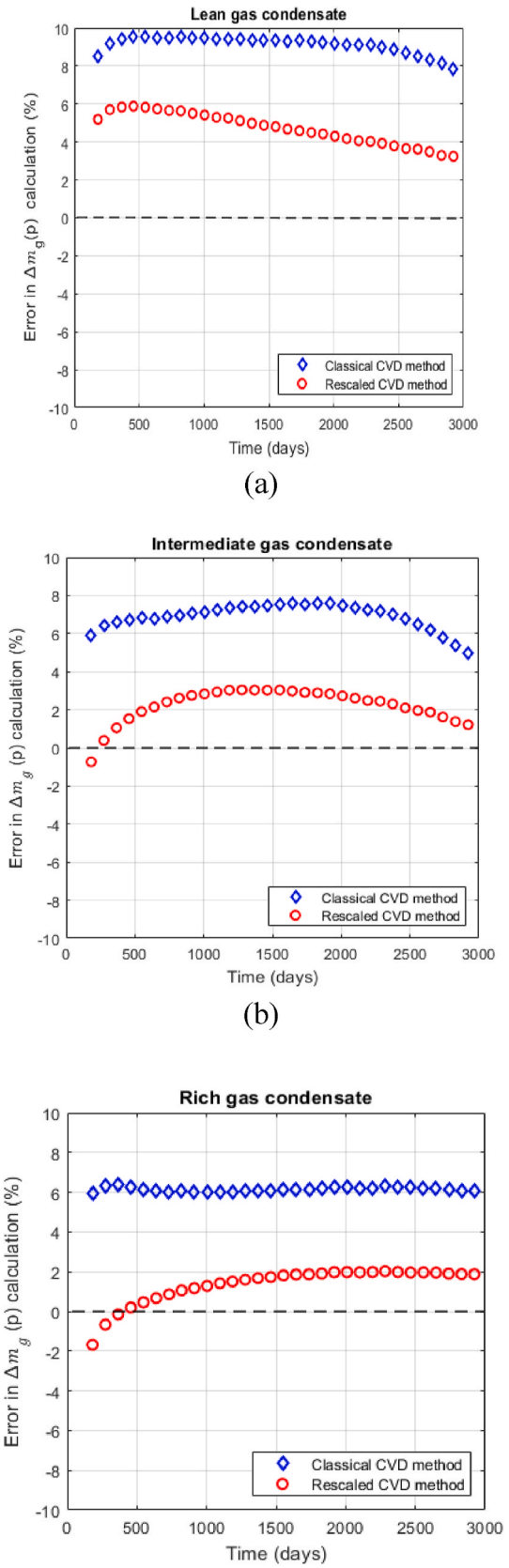

Fig. 10. Deviation in $\Delta m_g(p)$ calculation – constant BHP.

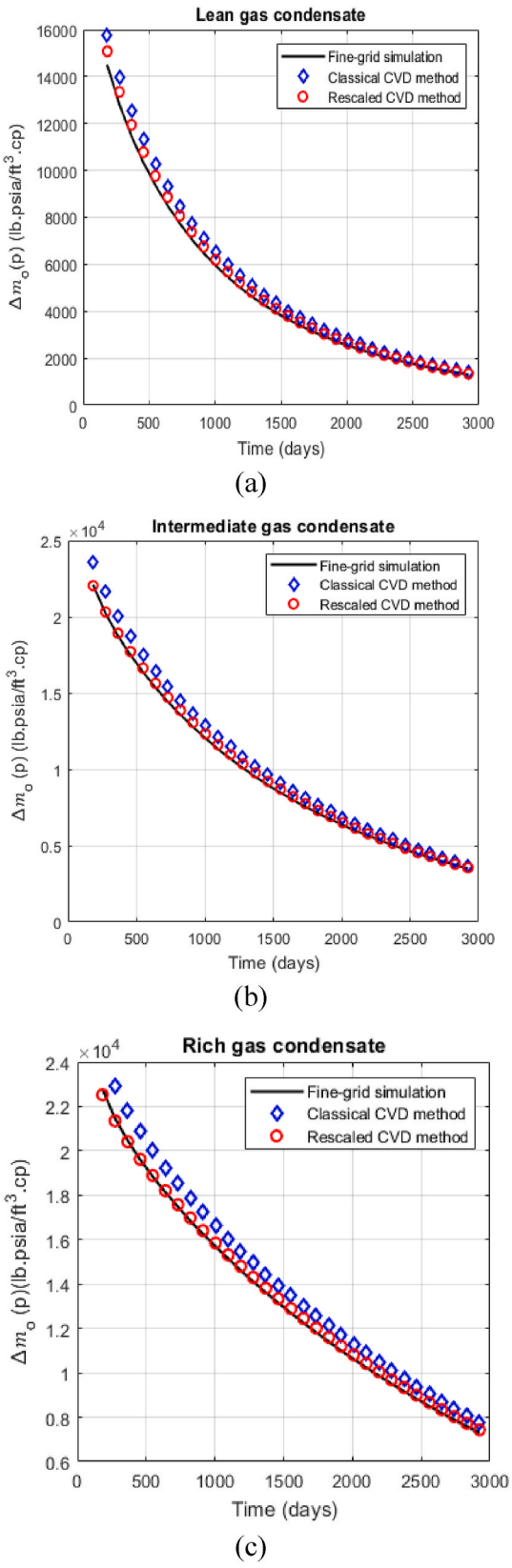

Fig. 11. $\Delta m_o(p)$ comparison – constant BHP.

To further establish the Rescaled CVD method as a reliable choice for multiphase pseudo-pressure calculation, it is consequential to extend the practicality of this method to several cases of operating constant bottomhole pressures. Arbitrary constant wellbore flowing pressures of

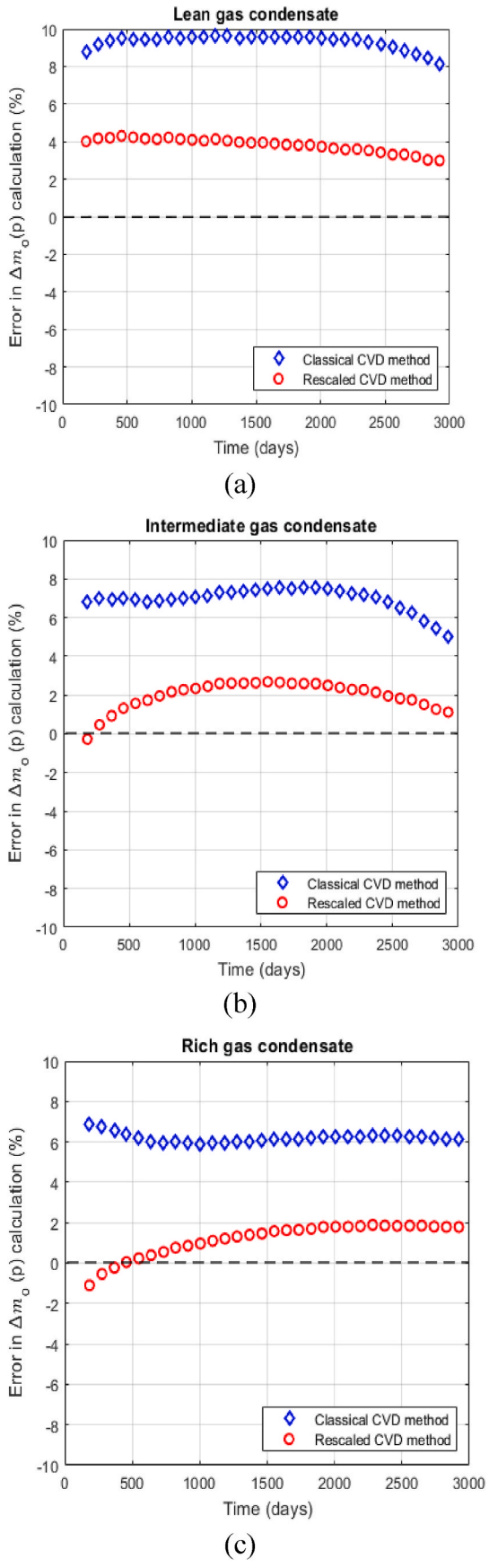

Fig. 12. Deviation in $\Delta m_o(p)$ calculation – constant BHP.

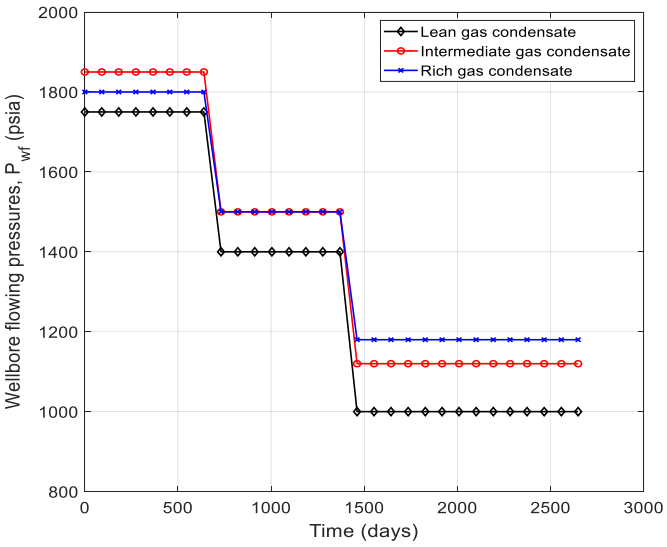

Fig. 13. Variable bottomhole pressure schedules.

1500 psia and 1350 psia are imposed on the numerical simulation exercise for each gas condensate case (for about 3000 days). The input reservoir parameters, fluid properties, relative permeability curves, and CVD data are derived from Appendix A. The production history and producing GOR for the gas condensate fluids producing under a constant BHP of 1500 and 1350 psia are provided respectively in Appendix C. Similarly, comparative results from these exercises showing the multiphase pseudo-pressure values for the surface gas and oil components for the three gas condensate cases are provided accordingly in Appendix C. Overall, the Rescaled CVD method still yields a better-estimating accuracy of multiphase pseudo-pressure as against the Classical CVD method.

The effectiveness of the Rescaled CVD method is also analyzed for more challenging production scenarios – varying bottomhole pressures. The variable bottomhole pressure schedules for all gas condensate systems are shown in Fig. 13. The input reservoir parameters, the production history and producing GOR are provided in Appendix D. The relative permeability curves and PVT data are the same as in the constant BHP case studies.

The comparative performance in multiphase pseudo-pressure estimations for the surface gas component in the distinct gas condensate fluids producing under varying BHP conditions are displayed in Figs. 14 and 15. Similarly, the compared estimates of multiphase pseudo-pressure values for the surface oil component are shown in Figs. 16 and 17. Results from the performance comparisons highlight the capability of the Rescaled CVD method in maintaining a better accuracy across the distinct gas condensate cases than the Classical CVD method. Unlike the classical approach, it is also observed that the Rescaled CVD method adapts to scenarios where increasing pressure drawdowns are encountered. Hence, the proposed S_o-p relationship could be considered as a robust tool for modeling gas condensate fluids producing under variable bottomhole pressure conditions.

5. Concluding remarks

This study presents an improved saturation-pressure relationship for boundary-dominated gas condensate reservoirs. The proposed approach offers a straightforward technique in mitigating potential errors in multiphase pseudo-pressure calculations in such complex natural gas systems. The FPM is a new parameter that identifies the inherent GOR behavior with respect to pressure particularly at and close to the transition interval of the steady-state region and the condensate build-up region. Using the GOR-pressure envelopes and relationships between $\frac{dGOR}{dp}$ and *FPM* show that the customary assumption of a constant GOR

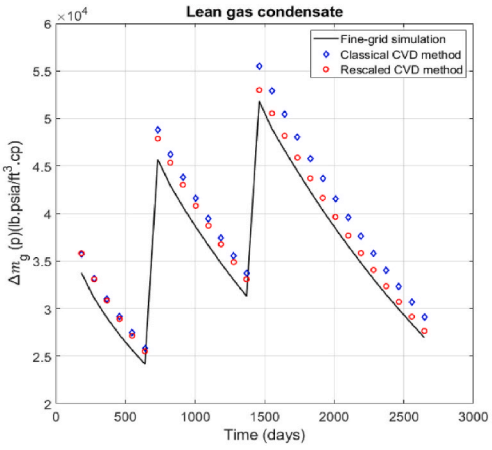

(a)

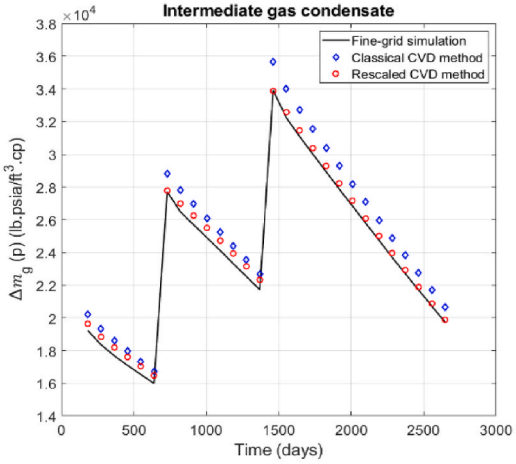

(b)

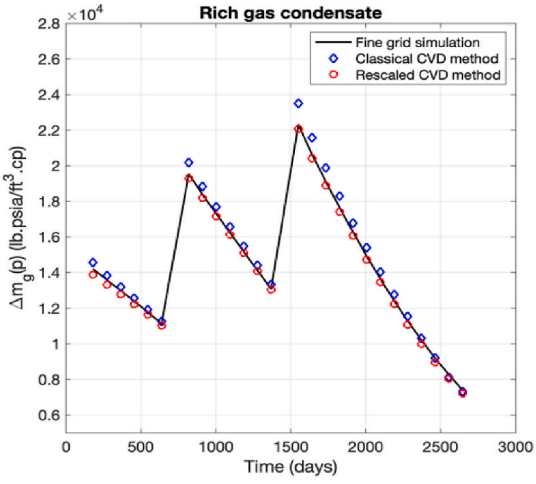

(c)

Fig. 14. $\Delta m_g(p)$ comparison – variable BHPs.

behavior in Region I should be revised. The p_1 determination protocol using FPM_{p_1} criterion is verified, thus reemphasizing that imminent departure from a constant GOR behavior becomes more pronounced within a range of FPM of 0.1–0.2 for the distinct gas condensate cases.

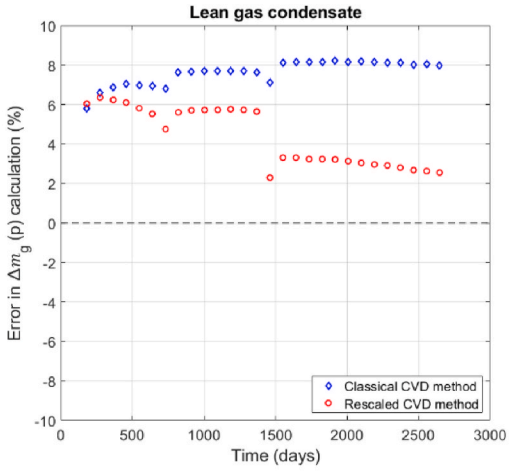

(a)

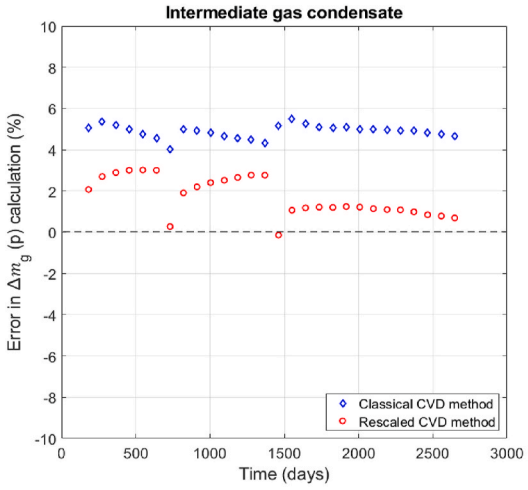

(b)

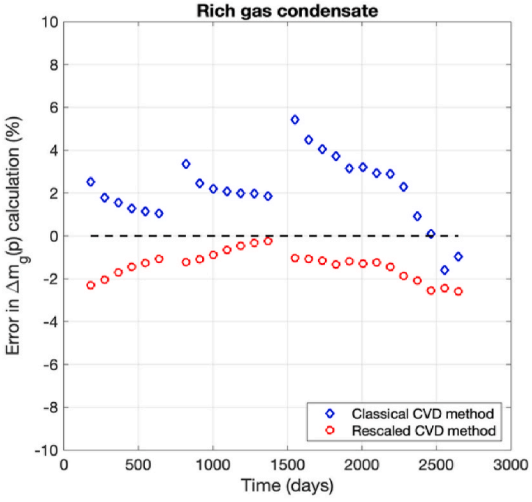

(c)

Fig. 15. Error in $\Delta m_g(p)$ calculation – variable BHPs.

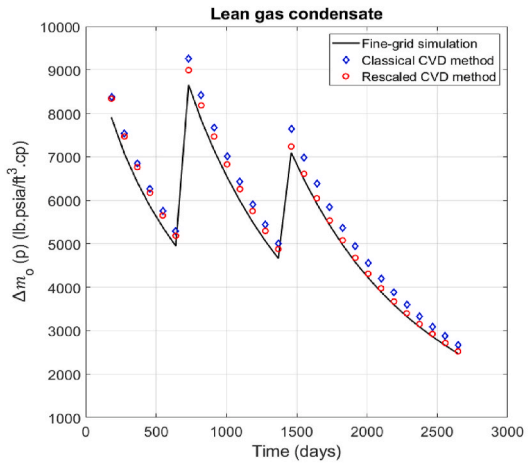

(a)

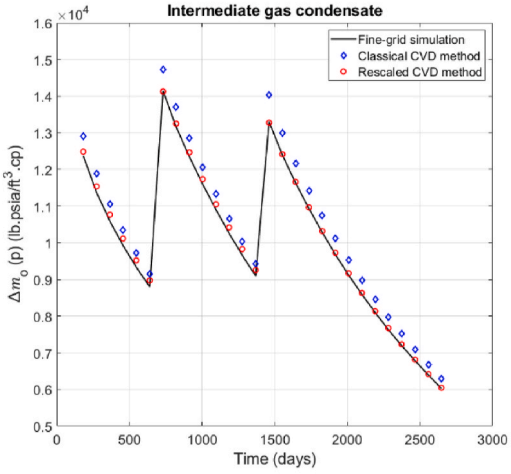

(b)

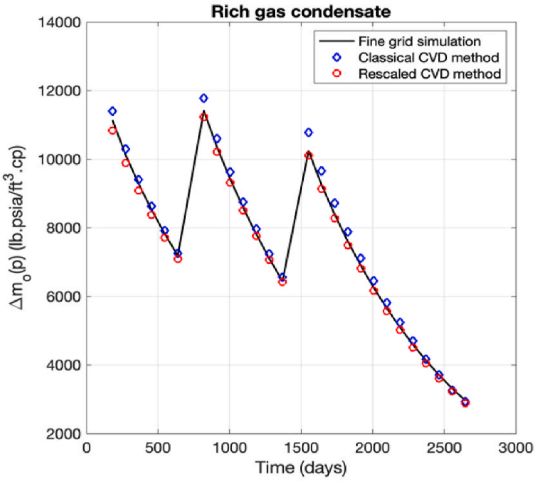

(c)

Fig. 16. $\Delta m_o(p)$ comparison – variable BHPs.

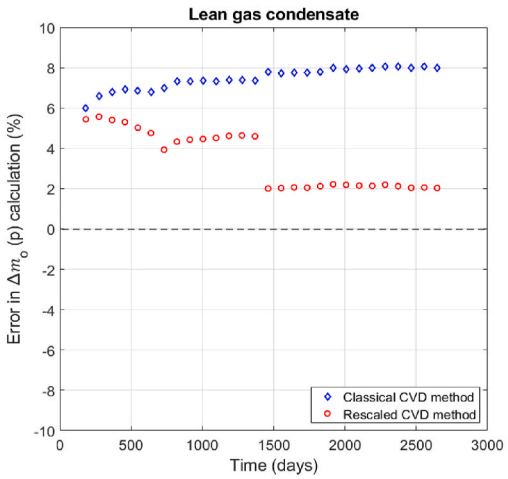

(a)

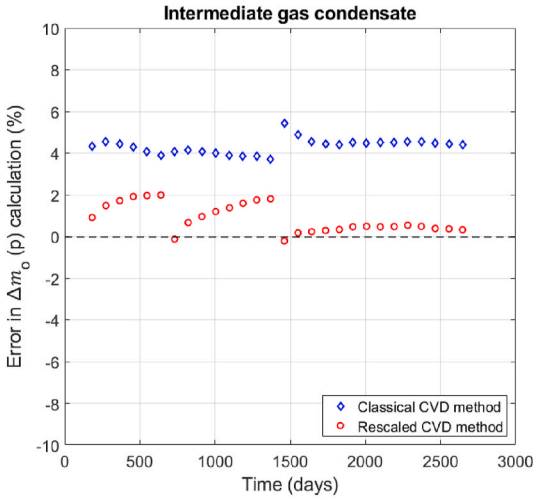

(b)

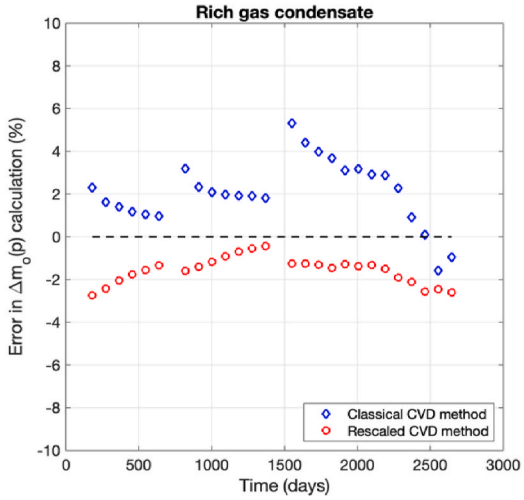

(c)

Fig. 17. Error in $\Delta m_o(p)$ calculation – variable BHPs.

However, sensitive analyses from preliminary inverse modeling and best flow rate predictions establish FPM of 0.2 as the most reliable criterion to determine the pressure value, p_1. Based on these observations, the conventional definition for the upper limit of the steady-state region (p^*) should be reconsidered since the signature behavior of steady-state flow (constant GOR) has been proven to depart prior to p^*. Coupling the FPM criterion with the Rescaled CVD approach, the robustness of the proposed method is emphasized through the effectiveness of multiphase pseudo-pressure calculations and the simplicity of its implementation protocol when subjected to constant and variable bottomhole pressure applications.

CRediT authorship contribution statement

Kien Tran: Writing – original draft, Validation, Methodology, Formal analysis, Conceptualization. **Bright Odike:** Writing – review & editing, Validation, Formal analysis, Data curation. **Jonathan Garcez:** Writing – review & editing, Supervision. **Luis F. Ayala H:** Supervision, Methodology, Conceptualization.

Declaration of competing interest

The authors declare that they have no known competing financial interests or personal relationships that could have appeared to influence the work reported in this paper.

Data availability

Data will be made available on request.

Nomenclature

Latin symbols

A	reservoir drainage area ft^2
B_g	gas formation volume factor ft^3/SCF
B_o	oil formation volume factor RB/STB
F_r	rescaling factor
h	formation thickness Ft
k	absolute permeability md
k_{ro}	relative permeability of oleic phase
k_{rg}	relative permeability of gaseous phase
$\Delta m_g\ (p)$:	multiphase pseudo-pressure of gas component lbm-psi/ft^3-cp
$\Delta m_o\ (p)$:	multiphase pseudo-pressure of oil component lbm-psi/ft^3-cp
Δm_{tp}:	multiphase pseudo-pressure of total component lbm-psi/ft^3-cp
p:	pressure psi
p^*	conventionally defined upper bound pressure for Region I psi
p_1	re-defined upper bound pressure for Region I psi
p_{dew}	dew-point pressure psi
p_i	initial pressure psi
p_{wf}	bottomhole or wellbore flowing pressure psi
$\bar{p}$:	average reservoir pressure psi
q_{gsc}	gas production rate at standard condition (14.7 psi, 60 °F) SCF/day
q_{osc}	oil production rate at standard condition (14.7 psi, 60 °F) STB/day
r_e	radius of the outer boundary of the system Ft
r_w	wellbore radius Ft
R_s	solution gas oil ratio SCF/STB
R_v	volatile oil gas ratio STB/SCF
S_o:	oil saturation
$S_{o,\bar{p}}$:	oil saturation at average reservoir pressure
S_{oc}:	critical oil saturation
$S_{o,CVD}$	oil saturation using CVD data
$S_{o.rescaled}$:	oil saturation using Rescaled CVD approach
$S_{o,wf}$:	oil saturation at bottom hole
t	time days
V_g:	volume of reservoir gas phase ft^3
V_o:	volume of reservoir condensate phase ft^3
$V_{ro,CVD}$:	fractional amount of liquid dropout in a CVD test - Greek symbols
α_c:	field unit conversion factor
φ	porosity - γ_g: mobility of gas phase lbm/ft^3-md
γ_{gsc}:	mobility of gas component lbm/ft^3-md
γ_o:	mobility of condensate phase lbm/ft^3-md
γ_{osc}:	mobility of oil component lbm/ft^3-md
μ_g:	gas viscosity md
μ_o:	oil viscosity md
ρ_g:	gas density lbm/ft^3
ρ_o:	oil density lbm/ft^3
ρ_{gsc}:	gas density at standard condition (14.7 psi, 60 °F) lbm/ft^3

ρ_{osc}: oil density at standard condition (14.7 psi, 60 °F) lbm/ft^3
ω_{Gg}: mass concentration of surface gas component in reservoir gas phase
ω_{Go}: mass concentrations of surface gas component in reservoir oil phase
ω_{Og}: mass concentration of surface oil component in reservoir gas phase
ω_{Oo}: mass concentrations of surface oil component in reservoir oil phase

Abbreviations

BDF	Boundary dominated flow
BHP	Bottomhole pressure
CEBO	Compositionally-extended black oil model
CMG	Computer Modeling Group Ltd
CVD	Constant volume depletion
EUR	Estimated Ultimate Recovery
FPM	Fractional phase mobility
GOR	Gas-oil ratio
IMEX	Implicit-explicit
LHS	Left hand-side
OGIP	Original gas in place
PDA	Production data analysis
PVT	Pressure-volume-temperature
RHS	Right hand-side

Appendix A. Fluid properties for gas condensate samples

Below are the fluid properties of gas condensate samples used in this study. The PVT data for these fluid systems are generated by our in-house phase behavior model.

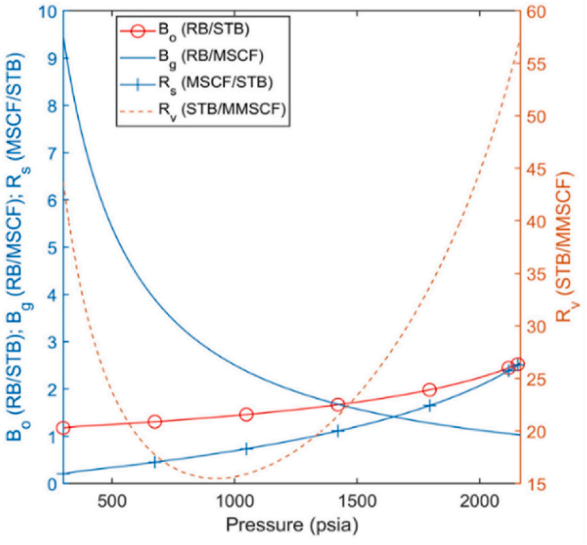

Fig. A-1. PVT data for lean gas sample.

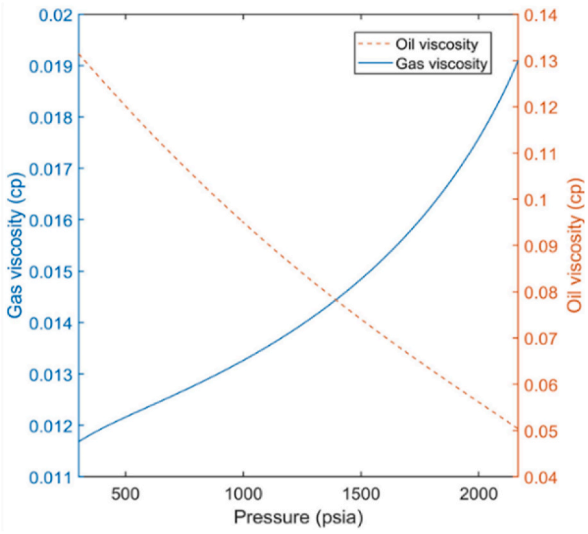

Fig. A-2. Viscosity data for lean gas sample.

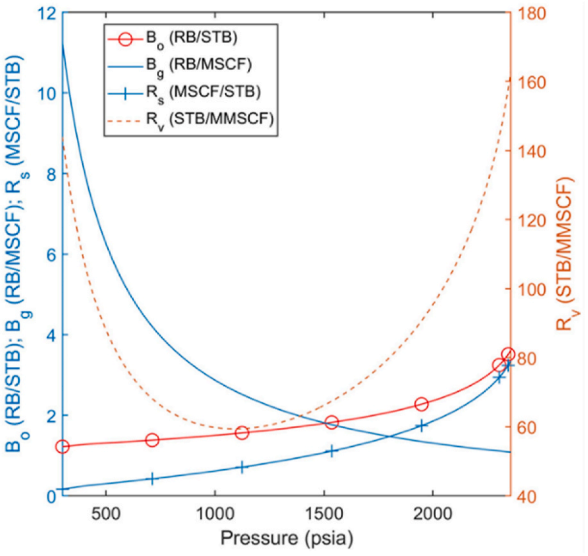

Fig. A-3. PVT data for intermediate gas sample.

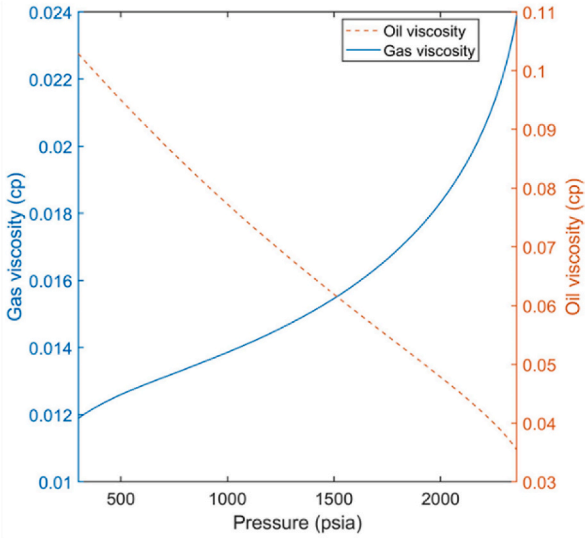

Fig. A-4. Viscosity data for intermediate gas sample.

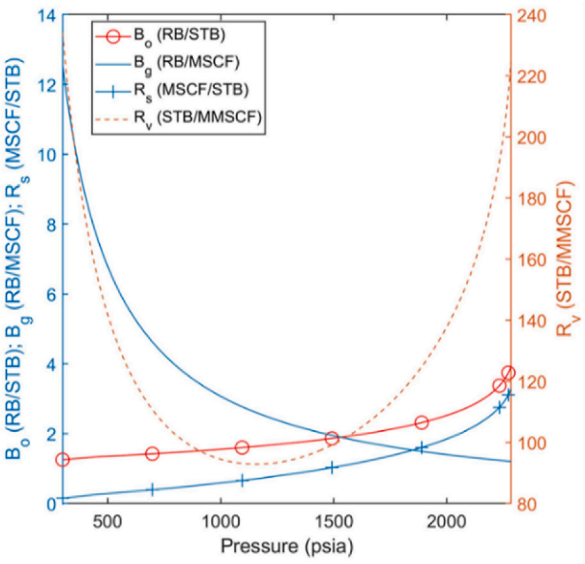

Fig. A-5. PVT data for rich gas sample.

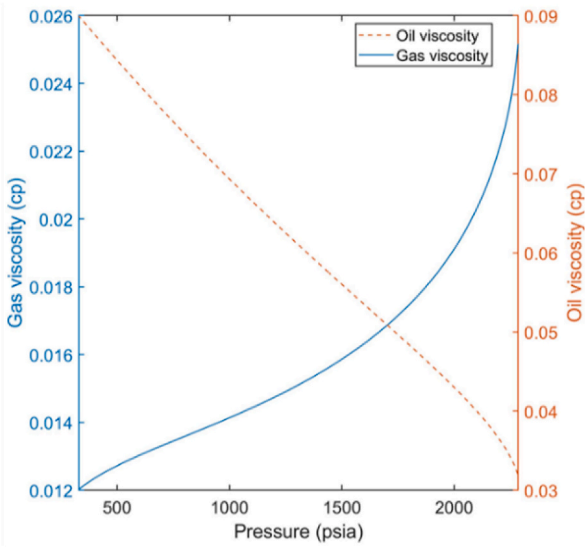

Fig. A-6. Viscosity data for rich gas sample.

Appendix B. Reservoir input and production history for gas condensate case studies

The input parameters for three gas condensate case studies (Case 1–3) are shown in Table B-1. Two sets of relative permeability data are utilized for the reservoir models for all case studies.

Table B-1
Input parameters for numerical simulation – case studies 1–3.

		Case 1 -lean gas	Case 2 - intermediate gas	Case 3 - rich gas
Reservoir temperature [F]	T	110	160	185
Initial pressure [psia]	p_i	2168	2358	2285
Bottomhole pressure [psia]	p_{wf}	1000	1120	1200
Reservoir boundary [ft]	r_e	3500	2500	2500
Wellbore radius [ft]	r_w	0.25	0.25	0.25
Pay zone thickness [ft]	h	50	50	50
Permeability [mD]	k	60	40	30
Porosity	φ	0.2	0.2	0.20
Critical oil saturation	S_{oc}	0.35	0.28	0.28
Oil density [lb/SCF]	ρ_{osc}	39.29	39.29	39.29
Gas density [lb/SCF]	ρ_{gsc}	0.0476	0.0476	0.0476
Original gas in place [MMCSF]	OGIP	66,700	32,251	29,127

In Fig. B-1, relative permeability set A was assigned to lean gas system and set B was assigned to intermediate and rich gas systems. Figs. B-2 and B-3 displays the production history of case1-3, including gas production rate and producing GOR versus time.

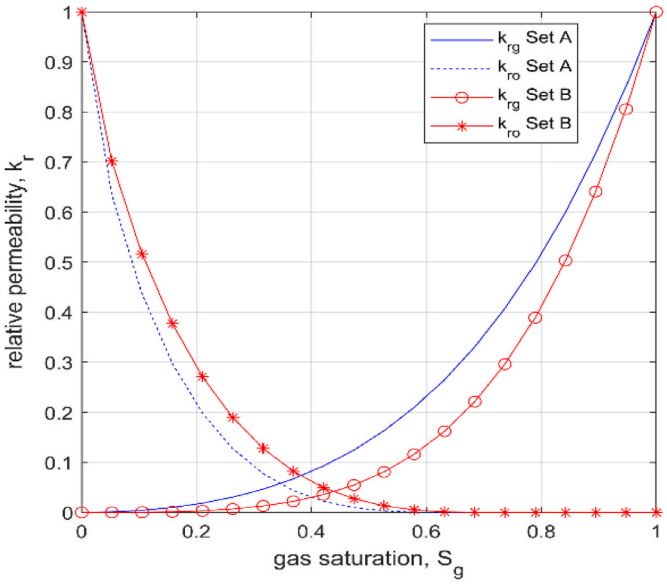

Fig. B-1. Relative permeability data sets.

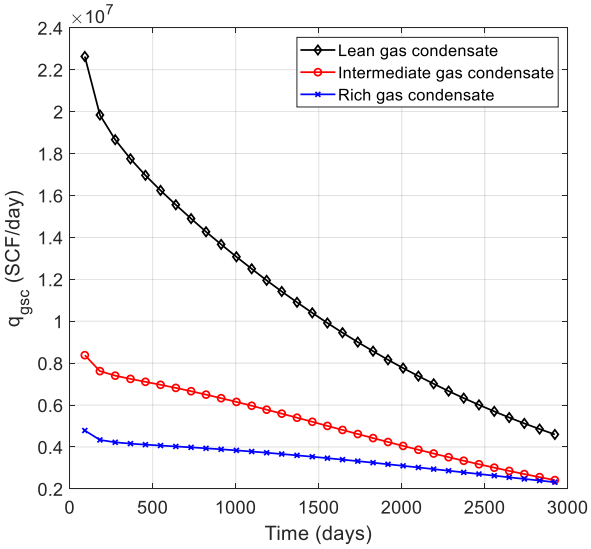

Fig. B-2. Gas production data for case studies 1–3.

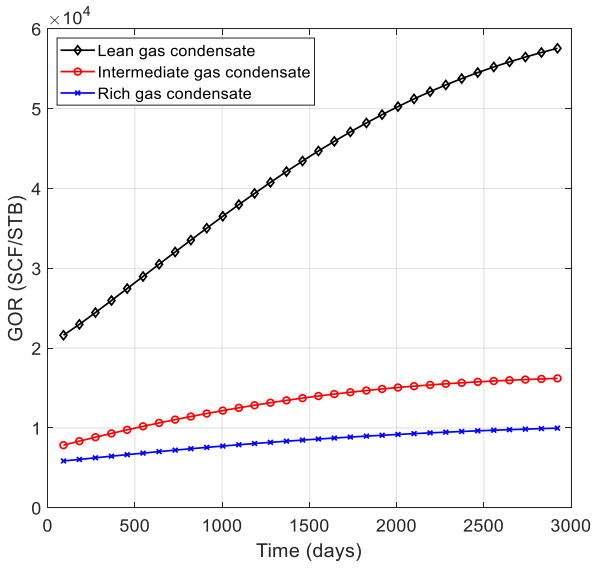

Fig. B-3. Producing GOR for case studies 1–3.

Appendix CMultiphase pseudo-pressure calculations (BHP of 1500 psia and 1350 psia)

Fig. C-1 presents $\Delta m_g(p)$ estimates for the gas condensate fluids producing at a constant BHP of 1500 psia.

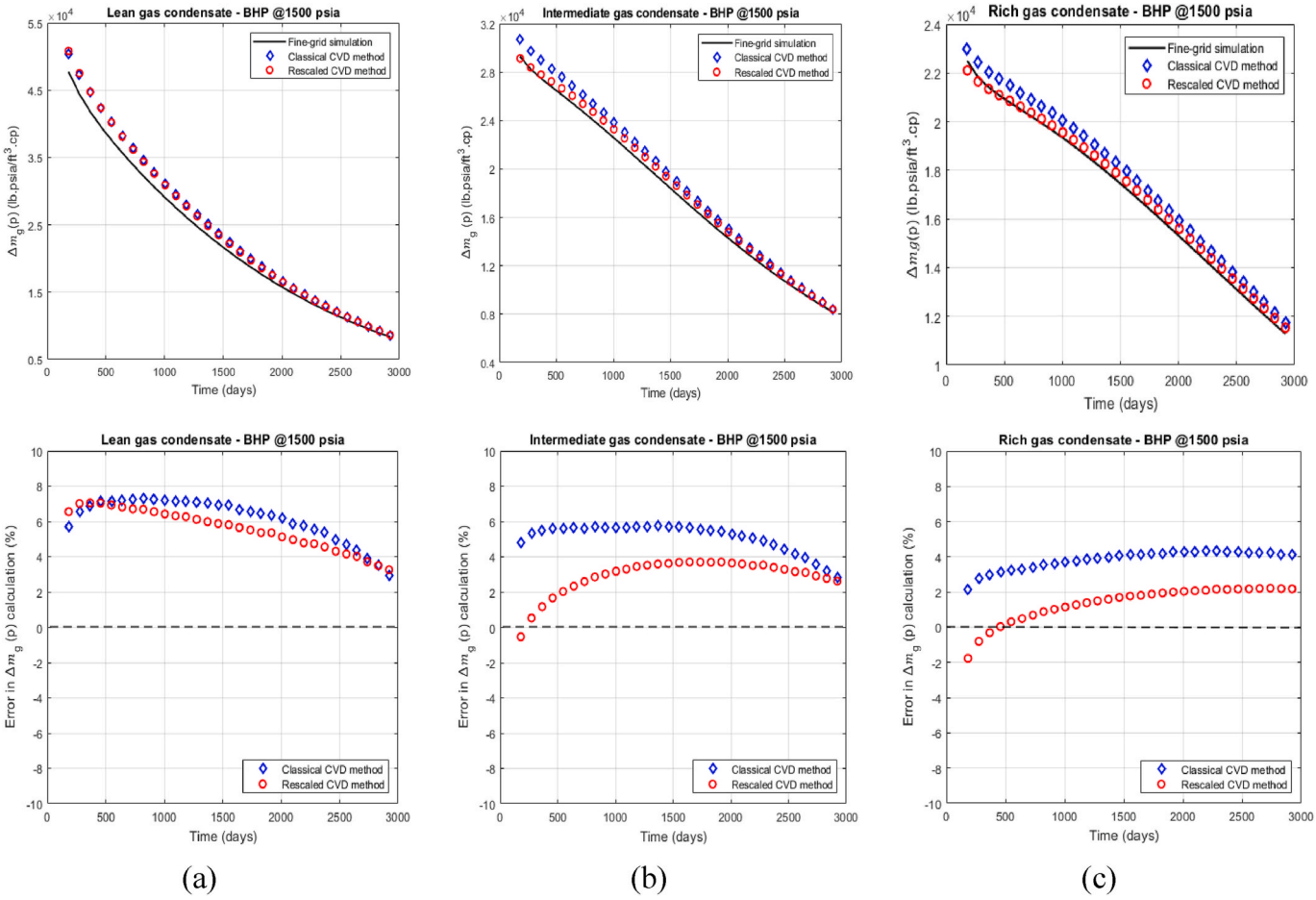

Fig. C-1. $\Delta m_g(p)$ Estimates and error in calculation (%) – BHP of 1500 psia.

Fig. C-2 presents $\Delta m_o(p)$ estimates for the gas condensate fluids producing under a constant BHP of 1500 psia.

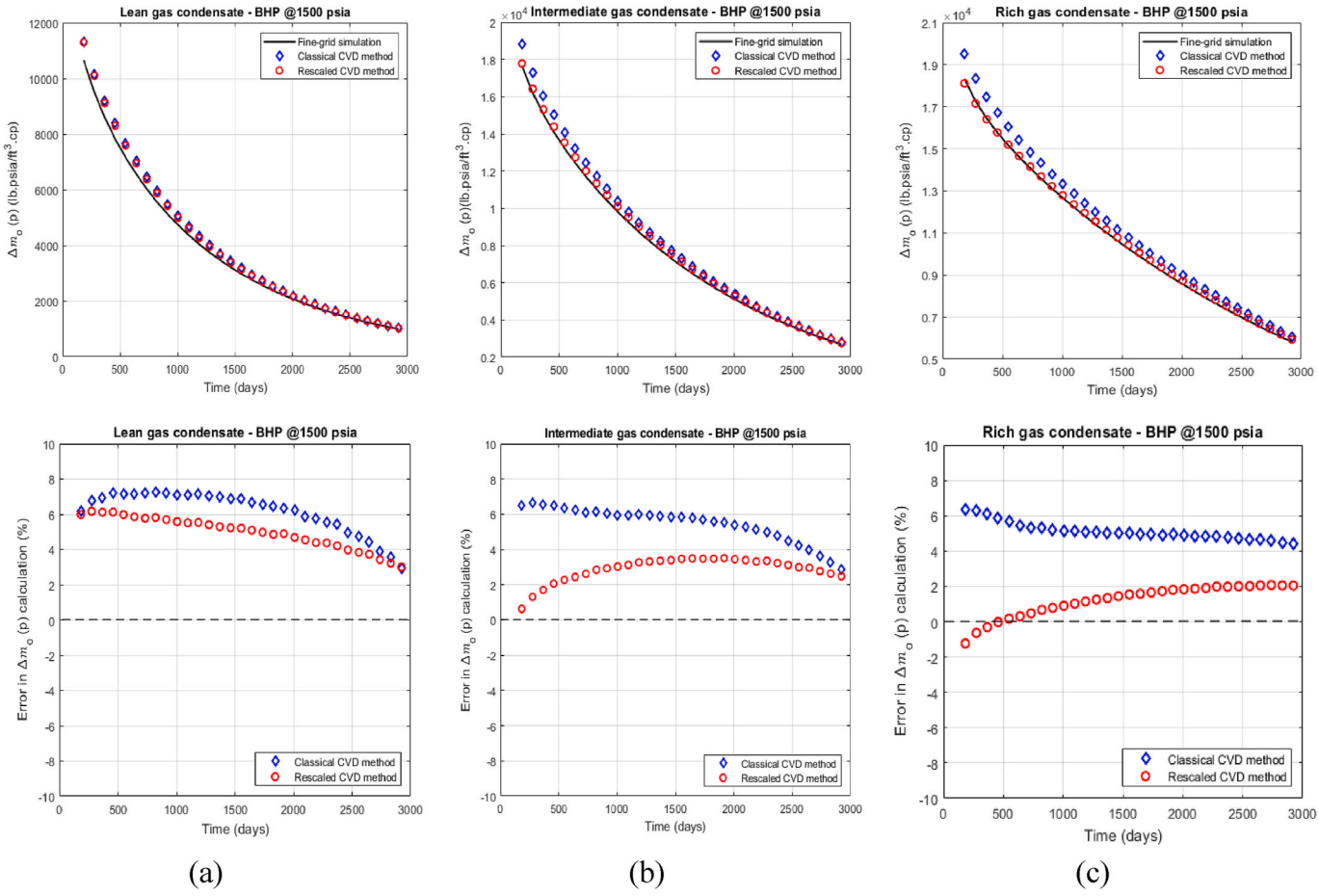

Fig. C-2. $\Delta m_o(p)$ Comparison and error in calculation (%) – BHP of 1500 psia.

Figs. C-3 and C-4 show the production history of the gas condensate fluids – BHP of 1500 psia.

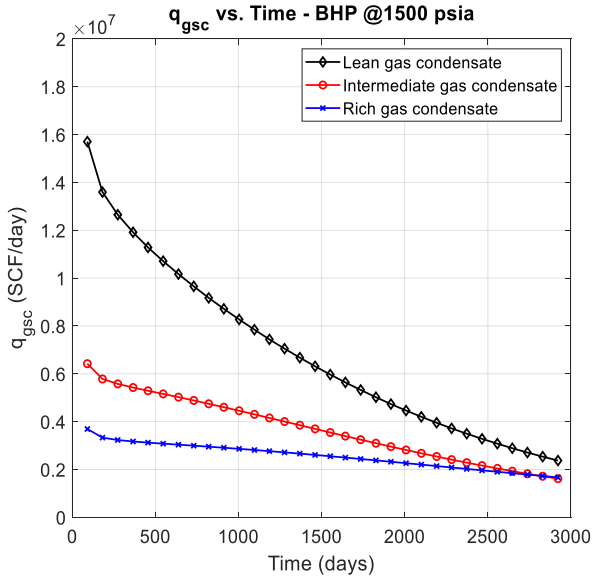

Fig. C-3. Gas production data - BHP of 1500 psia.

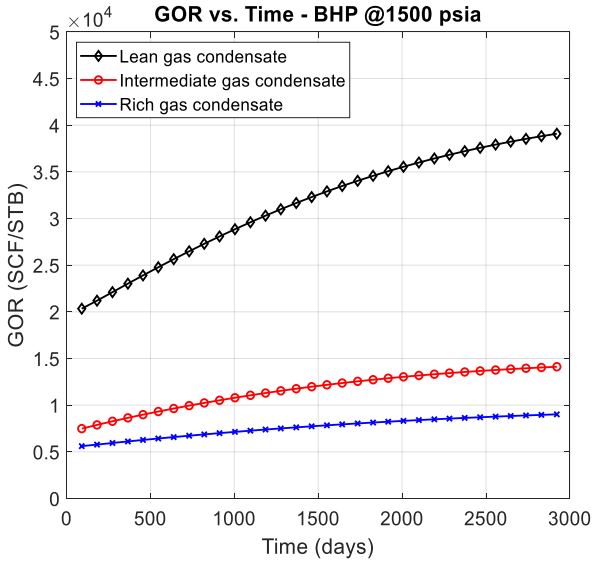

Fig. C-4. Producing GOR - BHP of 1500 psia.

Fig. C-5 presents $\Delta m_g(p)$ estimates for the gas condensate fluids producing under a constant BHP of 1350 psia.

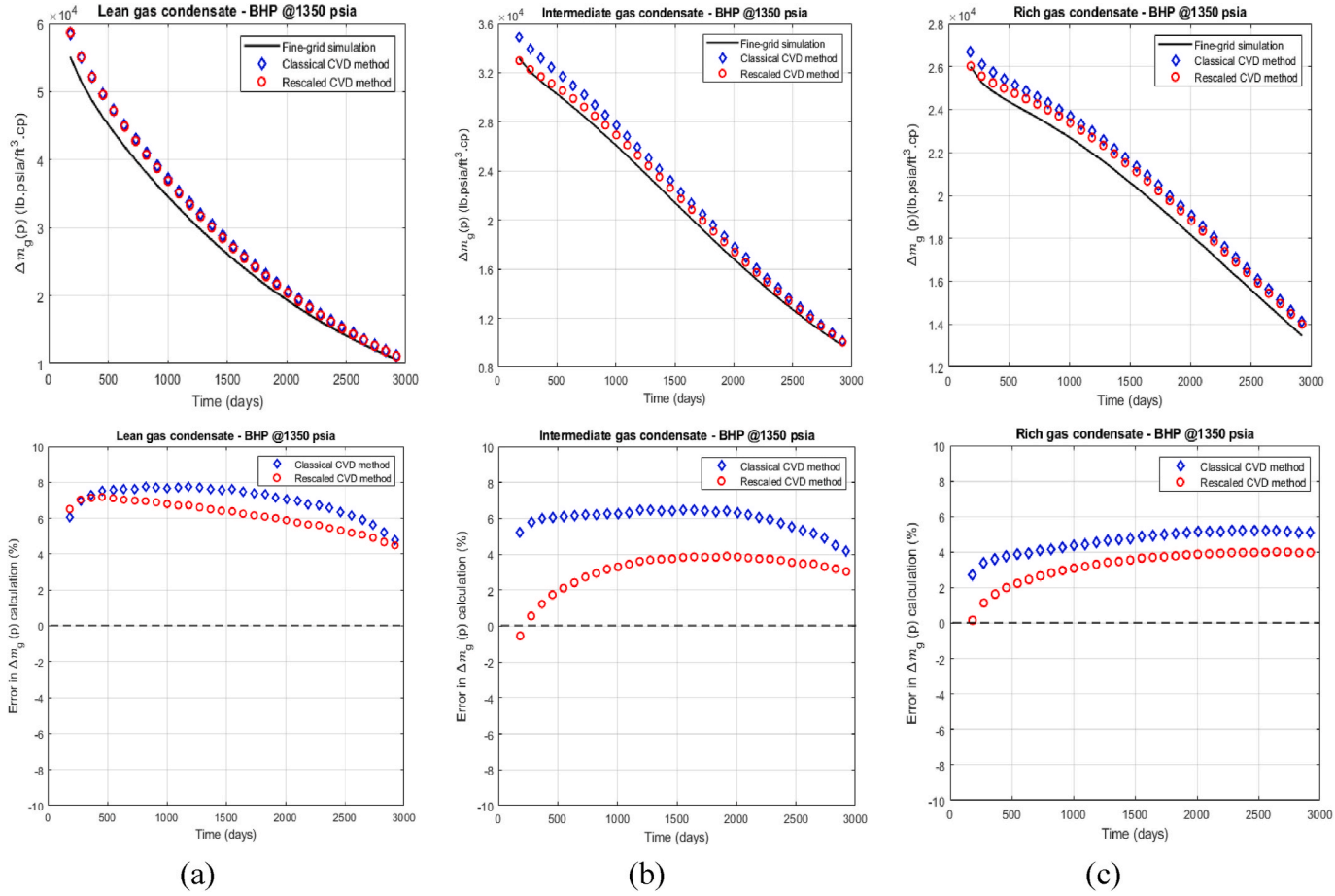

Fig. C-5. $\Delta m_g(p)$ Comparison and error in calculation (%) – BHP of 1350 psia.

Fig. C-6 presents the $\Delta m_o(p)$ estimates for the gas condensate fluids producing under a constant BHP of 1350 psia.

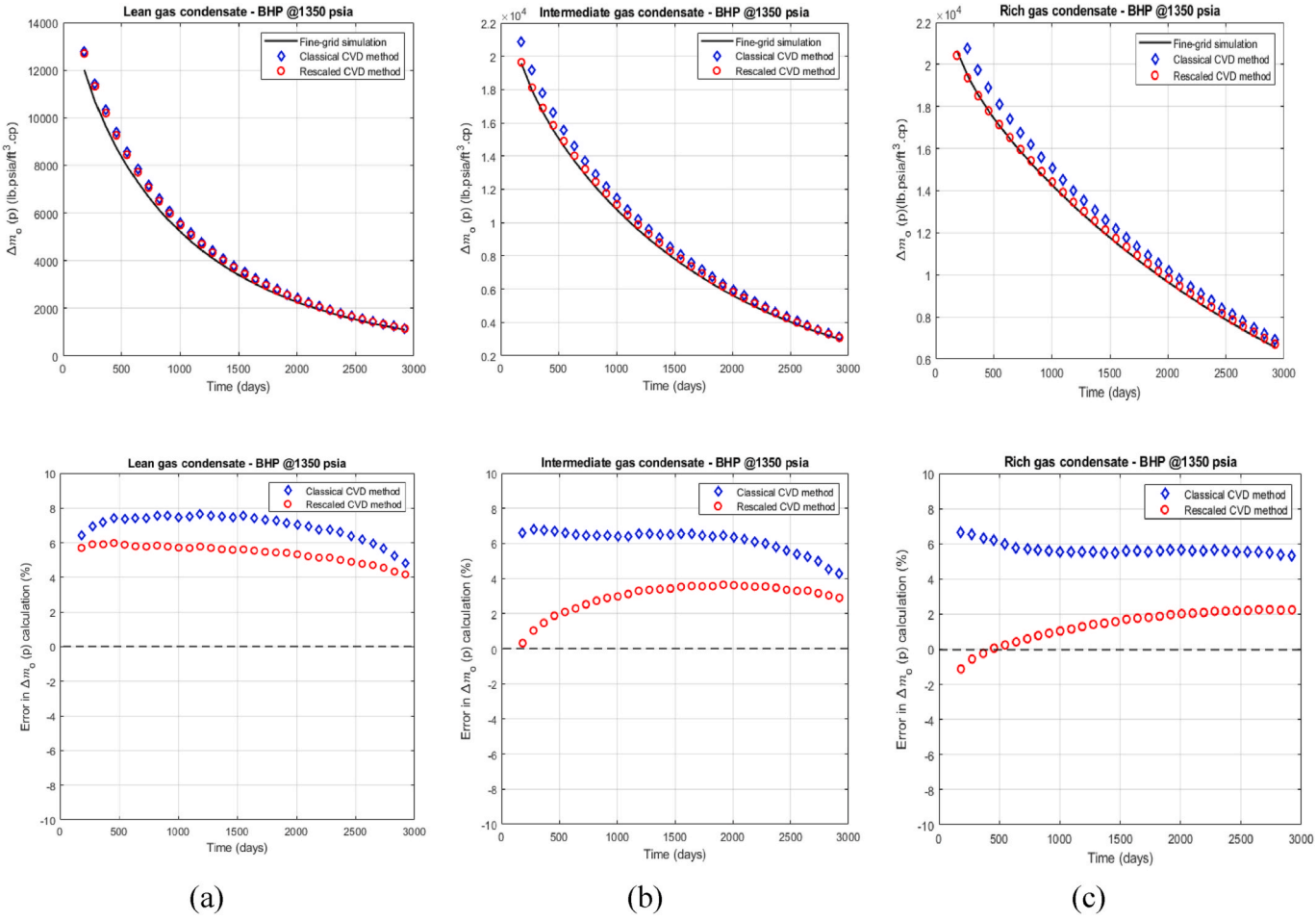

Fig. C-6. $\Delta m_o(p)$ Comparison and error in calculation (%) – BHP of 1350 psia.

Figs. C-7 and C-8 show the production history of the gas condensate fluids – BHP of 1350 psia.

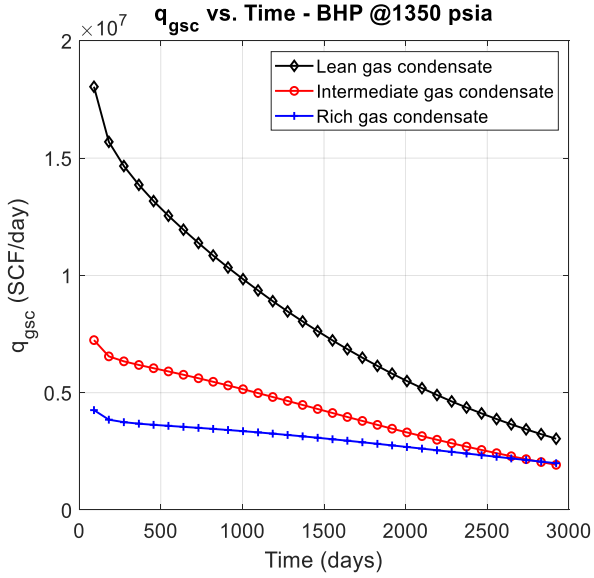

Fig. C-7. Gas production data - BHP of 1350 psia.

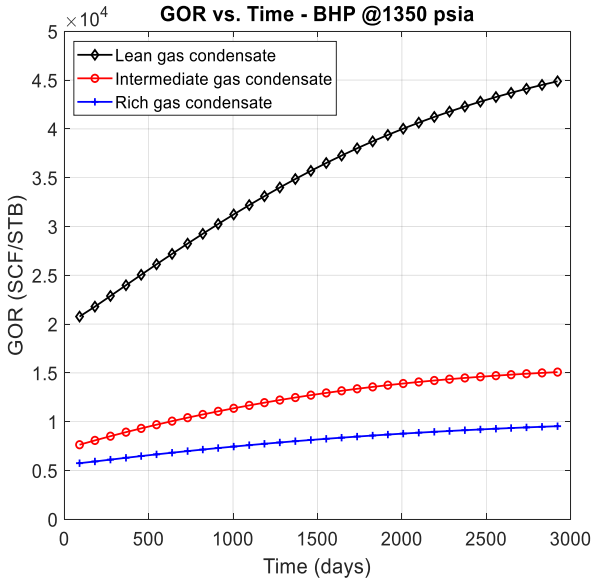

Fig. C-8. Producing GOR - BHP of 1350 psia.

Appendix D. Reservoir input and production history for gas condensate case studies 4–6

The input parameters for three gas condensate case studies (Case 4–6) producing under varying bottomhole pressures are shown in Table D-1. For variable bottomhole pressure scenarios, production schedule is set to be for about 2700 days (7–8 years) and the grid blocks assigned to the gas condensate cases are – lean gas ($900 \times 1 \times 1$), intermediate gas ($650 \times 1 \times 1$), and rich gas ($150 \times 1 \times 1$). The reservoir models are developed as finely discretized radial cylindrical grids of isotropic homogeneity under boundary-dominated flow with a vertical well in the center.

Table D-1
Input parameters for numerical simulation – case studies 4–6.

		Case 4 -lean gas	Case 5 - intermediate gas	Case 6 - rich gas
Reservoir temperature [F]	T	110	160	185
Initial pressure [psia]	p_i	2168	2358	2285
Reservoir boundary [ft]	r_e	3500	2500	1500
Wellbore radius [ft]	r_w	0.25	0.25	0.25
Pay zone thickness [ft]	h	50	50	50
Permeability [mD]	k	60	40	30
Porosity	φ	0.2	0.2	0.20
Critical oil saturation	S_{oc}	0.35	0.28	0.28
Oil density [lb/SCF]	ρ_{osc}	39.29	39.29	39.29
Gas density [lb/SCF]	ρ_{gsc}	0.0476	0.0476	0.0476
Original gas in place [MMCSF]	OGIP	66,700	32,251	13,158

Figs. D-1 and D-2 display the production history of all three gas condensate fluids producing under variable bottomhole pressure schedules.

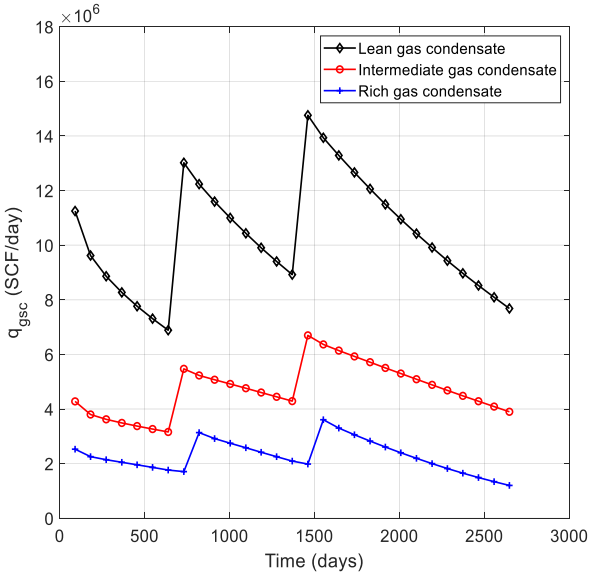

Fig. D-1. Gas production data for case studies 4–6.

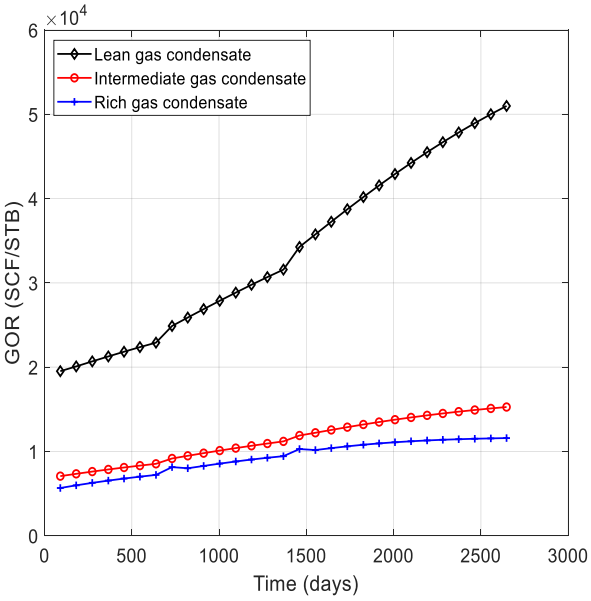

Fig. D-2. Producing GOR for case studies 4–6.

Appendix E. S_o-p Profile comparisons for all gas condensate case studies 1–6

At an arbitrary time-step (547 days), the S_o-p profiles are displayed in Fig. E-1. Notably, S_o-p profiles predicted by classical method using CVD data in Fig. E-1 shows substantial discontinuity at p^* because CVD test yields exceptionally low amount of liquid dropout in the pressure range of Region II. On the contrary, the S_o-p profiles predicted by the Rescaled CVD method indicated a smoother transition, while the discrepancy between the two emerged from the definition of upper pressure limit for the steady-state region (p^* in classical method and p_1 in the proposed approach).

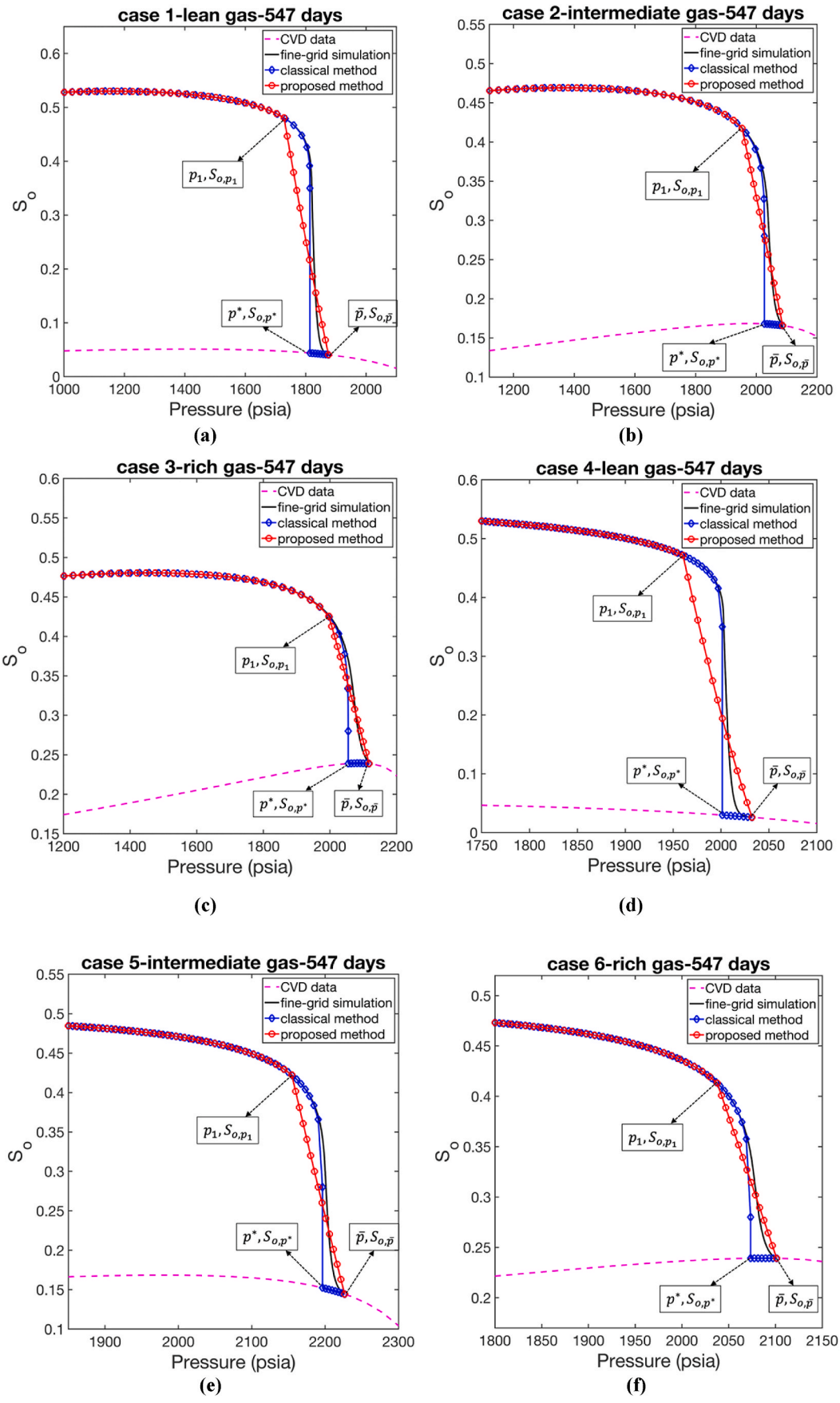

Fig. E-1. S_o-p Profiles comparison.

References

Agarwal, R.G., 1979. "Real gas pseudo-time"—a new function for pressure buildup analysis of MHF gas wells. All Days, SPE-8279-MS. https://doi.org/10.2118/8279-MS.

Al-Hussainy, R., Ramey Jr., H.J., Crawford, P.B., 1966. The flow of real gases through porous media. J. Petrol. Technol. 18 (5), 624–636. https://doi.org/10.2118/1243-A-PA.

Becker, M.D., Zhang, M., Ayala H, L.F., 2016. On the pressure-saturation path in infinite-acting unconventional liquid-rich gas reservoirs. J. Nat. Gas Sci. Eng. 35, 97–113. https://doi.org/10.1016/j.jngse.2016.08.007.

Behmanesh, H., Hamdi, H., Clarkson, C.R., 2015. Production data analysis of tight gas condensate reservoirs. J. Nat. Gas Sci. Eng. 22, 22–34. https://doi.org/10.1016/j.jngse.2014.11.005.

Behmanesh, H., Hamdi, H., Clarkson, C.R., 2017. Production data analysis of gas condensate reservoirs using two-phase viscosity and two-phase compressibility. J. Nat. Gas Sci. Eng. 47, 47–58. https://doi.org/10.1016/j.jngse.2017.07.035.

Behmanesh, H., Mattar, L., Thompson, J.M., Anderson, D.M., Nakaska, D.W., Clarkson, C. R., 2018. Treatment of rate-transient analysis during boundary-dominated flow. SPE J. 23 (4), 1145–1165. https://doi.org/10.2118/189967-PA.

Camacho, V., Raghavan, R., 1989. Inflow performance relationships for solution-gas-drive reservoirs. J. Petrol. Technol. 41 (5), 541–550. https://doi.org/10.2118/16204-PA.

Cheng, Y., Lee, W.J., McVay, D.A., 2008. Quantification of uncertainty quantification of uncertainty in reserve estimation from decline curve analysis of production data for unconventional reservoirs. J. Energy Resour. Technol. 130 (4) https://doi.org/10.1115/1.3000096.

Evinger, H.H., Muskat, M., 1942. Calculation of productivity factors for oil-gas-water systems in the steady state. Tran. AIME 146 (1), 194–203. https://doi.org/10.2118/942194-G.

Ertekin, T., Ayala, L.F., 2018. Reservoir Engineering Models: Analytical and Numerical Approaches. McGraw Hill LLC, United States.

Fetkovich, M.D., Guerrero, E.T., Fetkovich, M.J., Thomas, L.K., 1986. Oil and gas relative permeabilities determined from rate-time performance data. In: Proceedings - SPE Annual Technical Conference and Exhibition. https://doi.org/10.2523/15431-ms.

Fevang, Ø., Whitson, C.H., 1996. Modeling gas-condensate well deliverability. SPE Reservoir Eng. 11 (4), 221–230. https://doi.org/10.2118/30714-PA.

Jones, J.R., Raghavan, R., 1988. Interpretation of flowing well response in gas-condensate wells. SPE Form. Eval. 3 (3), 578–594. https://doi.org/10.2118/14204-PA.

O'Dell, H.G., 1967. Successfully cycling a low-permeability, high-yield gas condensate reservoir. J. Petrol. Technol. 19 (1), 41–47. https://doi.org/10.2118/1495-PA.

Panja, P., Velasco, R., Deo, M., 2020. Understanding and modeling of gas-condensate flow in porous media. Adv. Geo-Energy Res. 4 (2), 173–186. https://doi.org/10.26804/ager.2020.02.06.

Sun, Q., Ayala, L.F., 2020. Use of a new thermodynamics-based saturation/pressure relationship in two-phase rate-transient analysis of boundary-dominated gas/condensate reservoirs. SPE J. 25 (4), 1636–1656. https://doi.org/10.2118/201242-PA.

Sureshjani, M.H., Gerami, S., 2011. A new model for modern production-decline analysis of gas/condensate reservoirs. J. Can. Petrol. Technol. 50 (7), 14–23. https://doi.org/10.2118/149709-PA.

Walsh, M.P., Lake, L.W., 2003. A Generalized Approach to Primary Hydrocarbon Recovery, first ed. Elsevier.

Ye, P., Ayala H, F.L., 2012. A density-diffusivity approach for the unsteady state analysis of natural gas reservoirs. J. Nat. Gas Sci. Eng. 7, 22–34. https://doi.org/10.1016/j.jngse.2012.03.004.

Zhang, M., Ayala, L.F., 2014a. Gas-rate forecasting in boundary-dominated flow: constant-bottomhole-pressure decline analysis by use of rescaled exponential models. SPE J. 19 (3), 410–417. https://doi.org/10.2118/168217-PA.

Zhang, M., Ayala, L.F., 2014b. Gas-production-data analysis of variable-pressure-drawdown/variable-rate systems: a density-based approach. SPE Reservoir Eval. Eng. 17 (4), 520–529. https://doi.org/10.2118/172503-PA.

Zhang, M., Ayala, L.F., 2016. A density-based material balance equation for the analysis of liquid- rich natural gas systems. J. Pet. Explor. Prod. Technol. 6 (4), 705–718. https://doi.org/10.1007/s13202-015-0227-1.

Zhang, M., Ayala, L.F., 2017. Similarity-based, semi-analytical assessment of capillary pressure effects in very tight, liquid-rich gas plays during early-transient multiphase analysis. J. Nat. Gas Sci. Eng. 45, 189–206. https://doi.org/10.1016/j.jngse.2017.04.031.

Zhang, M., Ayala, L.F., 2019. A similarity-based semi-analytical solution for recovery performance assessment of unconventional oil and gas reservoirs with interfacial-tension-dependent capillary pressure effects. J. Energy Resour. Technol. 142, 42905 https://doi.org/10.1115/1.4044942.

Zhang, T., Li, Y., Sun, S., Bai, H., 2020. Accelerating flash calculations in unconventional reservoirs considering capillary pressure using an optimized deep learning algorithm. J. Petrol. Sci. Eng. 195, 107886 https://doi.org/10.1016/j.petrol.2020.107886.